12-5-95

SANDIA REPORT

SAND90–7084 • UC–721
Unlimited Release
Printed September 1995

Surface Complexation Modeling of Uranyl Adsorption on Corrensite from the Waste Isolation Pilot Plant Site

Sang-Won Park, James O. Leckie, Malcolm D. Siegel

Prepared by
Sandia National Laboratories
Albuquerque, New Mexico 87185 and Livermore, California 94550
for the United States Department of Energy
under Contract DE-AC04-94AL85000.

SF2900Q(8-81)

35

Issued by Sandia National Laboratories, operated for the United States Department of Energy by Sandia Corporation.

Available to DOE and DOE contractors from
Office of Scientific and Technical Information
PO Box 62
Oak Ridge, TN 37831

Prices available from (615) 576-8401, FTS 626-8401

Available to the public from
National Technical Information Service
US Department of Commerce
5285 Port Royal Rd
Springfield, VA 22161

NTIS price codes
Printed copy: A06
Microfiche copy: A01

SAND90-7084
Unlimited Release
Printed October 1995

Distribution
Category UC-721

Surface Complexation Modeling of Uranyl Adsorption on Corrensite from the Waste Isolation Pilot Plant Site*

Preliminary Potentiometric and Uranyl Adsorption Measurements

Sang-Won Park and James O. Leckie
Environmental Engineering and Science
Department of Civil Engineering
Stanford University
Stanford, CA 94305-4020

and

Malcolm D. Siegel
WIPP Chemistry and Disposal Room Systems
Sandia National Laboratories
Albuquerque, NM 87185

ABSTRACT

Corrensite is the dominant clay mineral in the Culebra Dolomite at the Waste Isolation Pilot Plant. The surface characteristics of corrensite, a mixed chlorite/smectite clay mineral, have been studied. Zeta potential measurements and titration experiments suggest that the corrensite surface contains a mixture of permanent charge sites on the basal plane and -SiOH and -AlOH sites with a net pH-dependent charge at the edge of the clay platelets. Triple-layer model parameters were determined by the double extrapolation technique for use in chemical speciation calculations of adsorption reactions using the computer program HYDRAQL. Batch adsorption studies showed that corrensite is an effective adsorbent for uranyl (UO_2^{2+}). The pH-dependent adsorption behavior indicates that adsorption occurs at the edge sites. Adsorption studies were also conducted in the presence of competing cations (Ca^{2+} and Mg^{2+}) and complexing ligands (CO_3^{2-}, ethylenediaminetetraacetic acid [EDTA] and oxine). The cations did not affect uranyl adsorption in the range studied (10^{-2} to 10^{-4} M). This observation lends support to the hypothesis that uranyl adsorption occurs at the edge sites. Uranyl adsorption was significantly hindered by carbonate in the concentration range 10^{-3} to 10^{-5} M. It is proposed that the formation of carbonate uranyl complexes inhibits uranyl adsorption and that only the carbonate-free species adsorb to the corrensite surface. The presence of the organic complexing agents EDTA and oxine also inhibits uranyl sorption; the effect of EDTA is greater than that of oxine.

*The work described in this report was performed for Sandia National Laboratories under Contract No. 05-4464.

ACKNOWLEDGMENTS

The authors thank Z. Lawson, J. H. Krumhansl (Sandia National Laboratories), and T. Sewards (University of New Mexico) for their assistance in the collection and characterization of the Waste Isolation Pilot Plant sample. We also thank C. Buehler for his assistance in the clay separation and B. Honeyman and M. Kohler for their assistance in several aspects of this study. C. F. Novak, T. E. Hinkebein, F. B. Nimick, D. B. Ward and M.T. Sautman provided technical reviews of this report.

CONTENTS

Figures

Tables

1.0 INTRODUCTION

1.1 Background

Assessment of the long-term fate of radionuclides disposed in deep geological repositories requires the identification and understanding of processes involved in the release or retention of radionuclides within likely geochemical settings. The transport, distribution, and fate of radionuclides in subsurface environments is known to be highly dependent on sorptive interaction with surrounding geomedia (Delegard and Barney, 1983; Franz et al., 1982; Rancon and Rochon, 1980). Sorption leads to a reduced aqueous concentration and a reduced rate of solute movement (Sargent and Vandergraaf, 1988; De Regge et al., 1988), which would directly influence the subsurface transport of radionuclides released from nuclear waste disposal sites. A better understanding of the basic chemical reactions of radionuclides at mineral/solution interfaces will contribute to both better insight into the environmental fate of these radionuclides and better estimation of radionuclide retardation in the subsurface environment.

Subsurface solids, both inorganic and organic, have surfaces with small unbalanced electrical charges, which attract ions from the aqueous phase (Grim, 1968; Van Olphen, 1977). The forces that bind these ions range from Van der Waals forces to chemical adsorption by valence bonds. The most effective adsorbing surfaces in the subsurface are clay minerals, zeolites, hydroxides of iron and manganese, humic substances, plant roots, microbial slimes, and microorganisms. Because interactions at interfaces are inevitable, it is important to assess the combined role of the various sorption and speciation processes on the retardation of radionuclides.

Much of the early work in this field was directed at determining the ratio of the radionuclide concentration on the solids to the total dissolved radionuclide concentration in water (Sanchez et al., 1982; Cranwell et al., 1987; Till and Meyer, 1983). This ratio, often referred to as a distribution coefficient, K_d, is used in transport codes to calculate the partitioning of radioelements between ground water and surrounding solids. The K_d is used to simulate the movement of radionuclides, but this model construct, although simple, is not appropriate for all aspects of radionuclide migration because the K_d, rather than being constant, is directly linked to solution composition and solid properties (Daniels et al., 1982; Sargent and Vandergraaf, 1988; Uematsu, 1988). The K_d is an empirical parameter that is a function of a number of variables, including radionuclide concentration, oxidation potential, ionic strength, pH, composition of the sorbing

surface and time (Sholkovitz, 1983). Figures 1-1 and 1-2 depict examples of the dependence of K_d values for U(VI) sorption on pH and carbonate ions, respectively.

In recent years, much effort has been invested in defining the partitioning of radionuclides between the aqueous phase and solid surfaces to avoid many of the ambiguities arising from use of the K_d concept and to better understand the chemical mechanisms involved in radionuclide transport. As an alternative to the K_d approach, a conceptually more rigorous model construct, the surface complexation models (SCMs) have been extensively studied (Davis and Leckie, 1978; Leckie and Tripathi, 1985; Park and Huang, 1989) including applications for radionuclide partitioning in geochemical settings (Kent et al., 1986; Hayes et al., 1990). The SCM is based on the assumption that a ligand exchange reaction may take place on the mineral surface, resulting in an inner-sphere complex between the surface functional groups and adsorbate ions (Huang and Stumm, 1973; Schindler et al., 1976). Because these SCMs incorporate various solution and surface chemical characteristics, this modeling approach has merit in its inherent flexibility in simulating a wide range of chemical scenarios. Several SCMs are discussed in Appendix A.

The triple layer model (TLM) version Davis and Leckie, 1978; James and Parks, 1982; Sposito, 1984; Hayes et al., 1990) of the SCM is used in this report. Simulation of adsorption with the TLM-SCM in a particular system requires specification of the physical-chemical properties of solids, such as the specific surface area, surface site density, surface charge and surface ionization constants; and the solution chemistry of the adsorbate and interacting species, including the chemical speciation through hydrolysis, complexation, oxidation/reduction in the absence and/or presence of various ligands, and oligomerization.

Modeling adsorption data with the TLM-SCM requires a serious evaluation of the quality of the experimental data and obtaining a data set that extends over a broad range of experimental conditions. The process of fitting a data set to the model provides a structured means of evaluating the quality and quantity of the data. The methodologies for collecting and modeling adsorption data, and defining constraints on simulations with verified models are bound together in the SCM approach. Several steps are involved in applying the SCM approach to describing adsorption. The adsorption properties of the substrate must be characterized. The best available thermodynamic data for the formation of solution complexes involving the adsorbate must be collected and corrected to the appropriate standards and reference states. Adsorption studies must be carried out over the widest possible range of experimental conditions. Stoichiometries and binding constants for surface complexes that give the best fit to the experimental data over the range of suspension compositions studied must be determined.

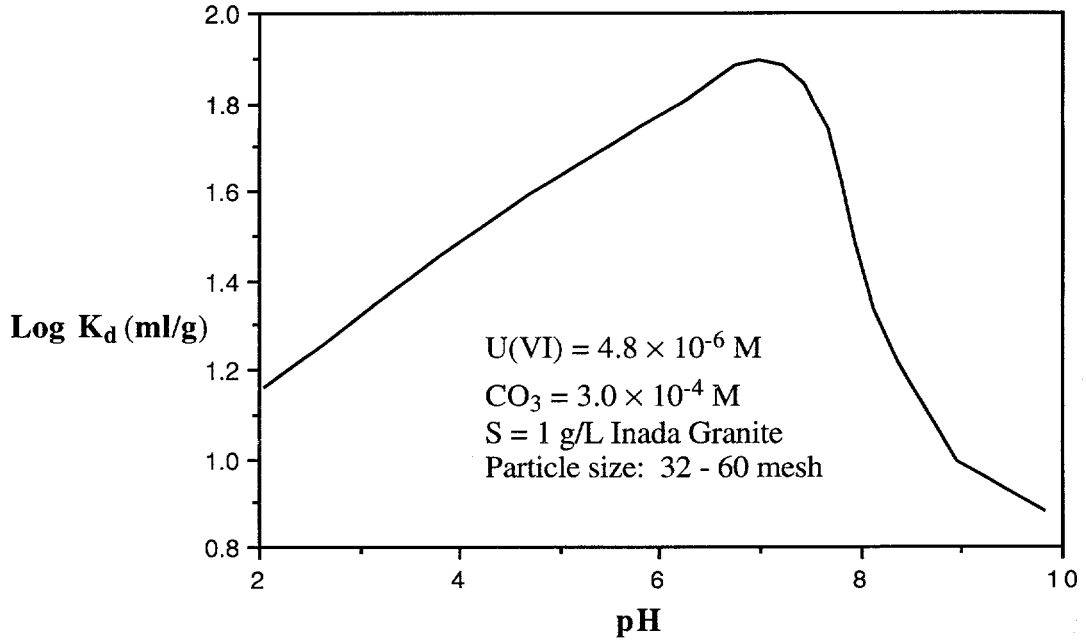

Figure 1-1. Distribution coefficient of U(VI) for Inada granite as a function of pH (after Sakamoto as cited in Uematsu, 1988).

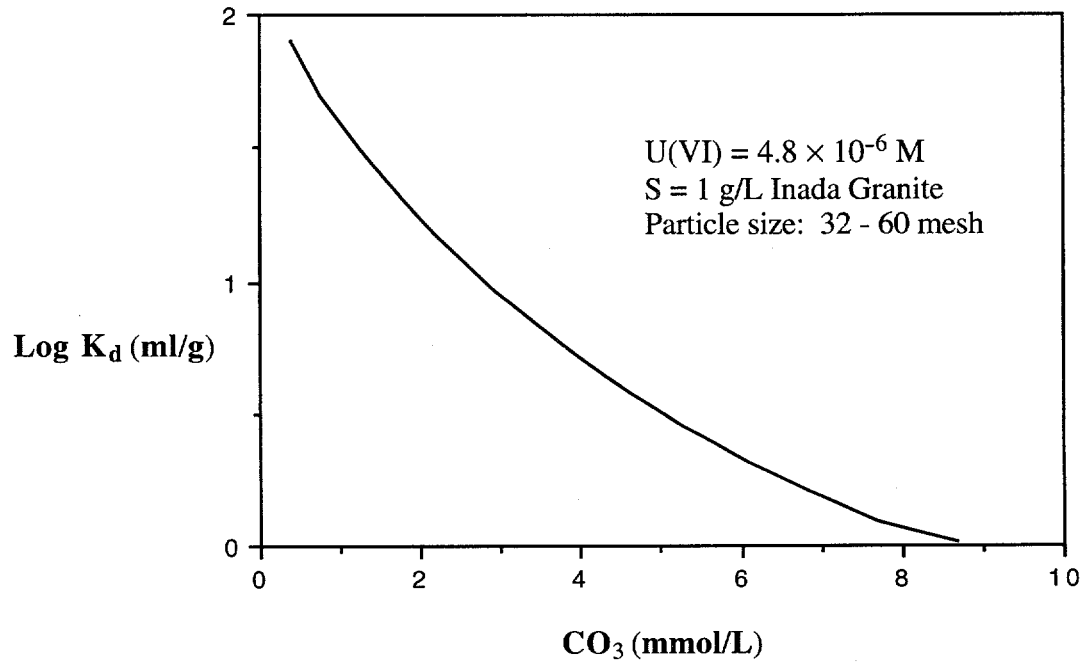

Figure 1-2. Distribution coefficient of U(VI) for Inada granite as a function of carbonate concentration (after Sakamoto as cited in Uematsu, 1988).

1.2 Description of the Waste Isolation Pilot Plant

The Waste Isolation Pilot Plant (WIPP) in Southeastern New Mexico is being studied for the geological disposal of defense-generated transuranic (TRU) wastes. Figure 1-3 shows the location of the WIPP site relative to the Northern Delaware Basin. Figure 1-4 provides a generalized stratigraphy of the Ochoan (Permian) rocks in the vicinity of the WIPP. The repository has been constructed within the Salado Formation, a thick Ochoan evaporite formation. The Culebra Dolomite Member of the Rustler Formation, a thin (10 m) fractured dolomite aquifer lies approximately 450 m above the repository horizon. This unit is the most likely pathway for long-term migration of radionuclides to the accessible environment in the event of a breach of the repository.

1.2.1 Radionuclide Release Scenario

Initial performance assessment calculations (Lappin et al., 1989; Marietta et al., 1989) indicate that releases of plutonium and uranium might dominate the radiological and chemical discharges from the WIPP to the environment. The calculations indicate that significant discharges of radionuclides may occur if the repository and a pressurized brine pocket in the underlying Castile Formation are intruded by a borehole after final emplacement of the waste.

Mixing of emplaced wastes with fluids from the Castile and Salado Formations and the Culebra Member would control the chemistry of the radionuclide-bearing brine as it enters the Culebra. Interaction of the water with rocks along the flow path may further alter the solution chemistry (Siegel, 1990). At the present time, the salinities of water in the Culebra range from <10,000 to >200,000 mg/L within the WIPP site. The concentrations of the major solutes (Cl, SO_4, Mg, Ca, K) as well as the Mg/Ca ratio are correlated with Na concentration (Siegel et al., 1991). The Salado Formation contains small amounts of Mg-Na-Cl rich brines (TDS = approximately 380,000 mg/L; Lappin et al., 1989). The brine pockets in the Castile contain Na-Cl brine [Total Dissolved Solid (TDS)= approximately 350,000 mg/L; Popeliak et al., 1983].

Radionuclide/clay interactions may be an important mechanism of radionuclide retardation. The amount of radionuclide sorption within the Culebra will be strongly dependent upon solution chemistry and the nature of the minerals that are exposed to the solutions. Collection of experimental data that can be used to simulate the degree of uranium sorption over a wide range of solution compositions is a prerequisite to performance assessment calculations.

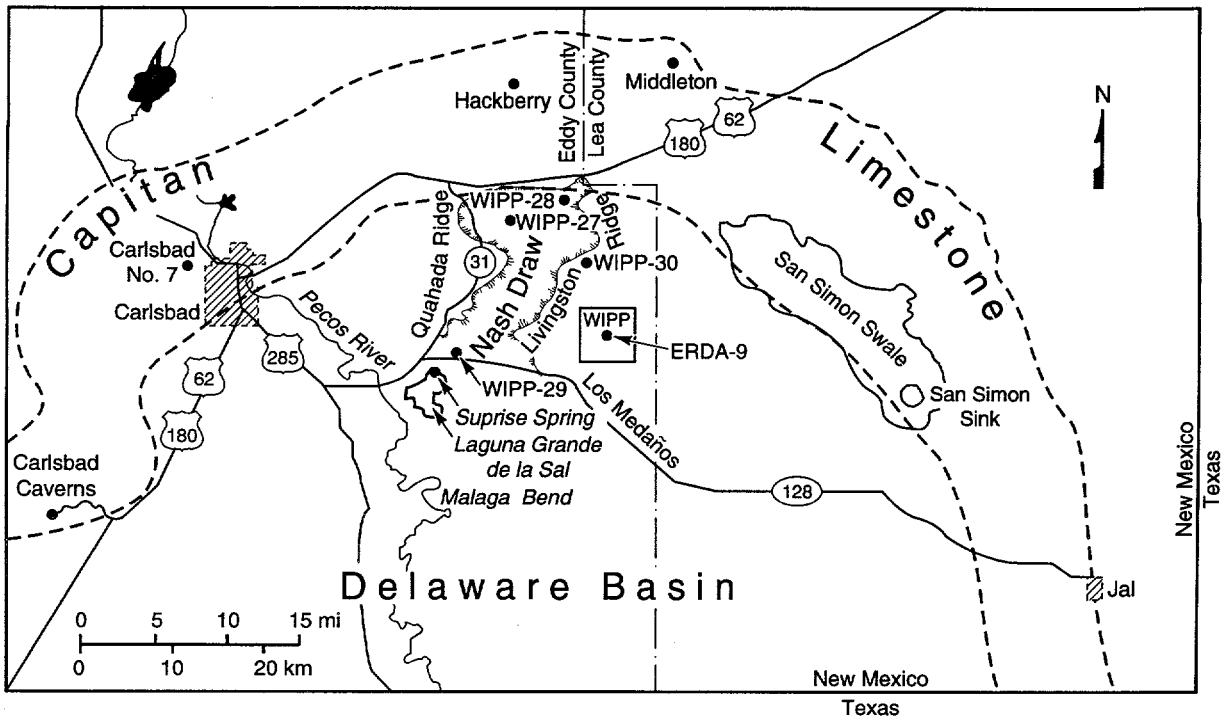

Figure 1-3. Setting of the WIPP Site relative to northern Delaware Basin and location of samples sites mentioned in this report.

OCHOAN	DEWEY LAKE RED BEDS	
	RUSTLER	Forty-niner
		Magenia Dolomite
		Tamarisk
		Culebra Dolomite
		Unnamed
	SALADO	
	CASTILE	

Figure 1-4. Generalized stratigraphy of Ochoan (Permian) rocks in the vicinity of the WIPP Site.

1.2.2 Mineralogy along Potential Radionuclide Transport Paths

The dominant mineral in the Culebra Member is a fairly pure dolomite that comprises about 85 percent by weight of the bulk rock (Sewards et al., 1991). Clay minerals comprise 1 to 10 weight percent of the bulk rock and 1 to 43 weight percent of the fracture-lining material (Sewards, 1991). Within the matrix, the clay occurs as disseminated particles and thin layers. In the most transmissive parts of the Culebra, fluid flow may be controlled by fractures (Lappin et al., 1989). Gypsum ($CaSO_4 \cdot 2H_2O$), and clays are the most abundant fracture-fill minerals (Sewards et al., *1991*; Sewards, 1991). Horizontal fractures within the Culebra may form in response to stresses induced by dissolution of underlying salt beds and occur along zones where clay is concentrated. The clay appears to represent primary horizontal bedding planes. The most commonly occurring clay minerals are (in order of abundance) corrensite (an ordered saponite/chlorite mixed clay) > illite > chlorite > serpentine.

Clays are also present in mudstone layers within the Tamarisk and unnamed members of the Rustler Formation. Corrensite-rich samples from a black shale and a red shale layer directly underlying the Culebra have been obtained from drill holes and shafts (Sewards et al., 1992). Because only small amounts of clay can be sampled from the Culebra fracture coating, initial technique and model development for the sorption studies were carried out with a reference corrensite (CorWa) and a corrensite sample (CorWIPP; sample ID: AIS-15) from the black shale layer sampled in the Air Intake Shaft (AIS). The distribution and composition of corrensite within several formations at the WIPP Site have been studied by Sewards et al. (1992) and Krumhansl et al. (1990). These studies are summarized in Appendix B and provide the basis for comparison of the properties of the corrensite in the Culebra with the samples from the AIS.

1.3 Scope

This study will improve understanding of specific adsorption mechanisms under relatively well-defined conditions and provide data for the interpretation of transport experiments and natural analogues. Without such data, conclusions from such experiments may be ambiguous. In practice, these two aspects are often related because parameters derived from experiments may be model-dependent, and an interpretation of experiments with inadequate models leads to unreliable parameter values and wrong conclusions.

This work provides a preliminary data set describing the adsorption of uranium by corrensite in solutions with low ionic strength. The study also examines the physical and chemical characteristics of the clay that are important to understanding the adsorption of uranium. It provides an overview of all aspects of collecting and modeling adsorption data using the triple-layer surface-complexation model in well-characterized systems.

2.0 EXPERIMENTAL METHODOLOGY

2.1 Preparation of the WIPP Sample and Its Characterization

The WIPP sample (CorWIPP; sample ID: AIS-15) was disaggregated with the help of a high intensity ultrasonic processor, Vibra Cell Model VC600 (Sonics & Materials, Inc.). The ultrasonic processor was run for 10 hr with the sonic probe dipping into 1L Milli-Q water containing 20 g of raw material. Due to the heat generated by the sonic probe, the sonicator was operated at 20-minute intervals with 80% duty cycle in an intermittent operation mode (10-minute cooling period). The fine particles produced by the ultrasonic process were analyzed by X-ray diffraction (XRD) for crystallinity and structure at Sandia National Laboratories (SNL) as described in Appendix B (Figure 2-1). A standard corrensite sample (CorWa) obtained from the Clay Mineral Society Source Clay Repository was also analyzed by XRD at Stanford using a Picker 1 Quarter Circle Diffractometer (Figure 2-2). Smear paste specimens of the clay were prepared and analyzed for identification. As shown in Figures 2-1 and 2-2, the diffractograms show a clear corrensite pattern. In general, there appears to be no important mineralogic differences between the CorWa and the CorWIPP. Both samples consist primarily of corrensite, with small amounts of quartz, illite, and subordinate clinochlore. It also appears that the proportions of these various components are about the same in each sample. The energy dispersive spectra of the sample showed Si> Mg> = Al, and that the clay contained traces of K and Fe.

One of the most important physical characteristics with respect to surface chemical reactions of natural soils or clays is the specific surface area (S_A). The corrensite samples were analyzed for specific surface area by the BET (Brunauer, Emmett, and Teller) method (Gregg and Sing, 1982). The BET gas adsorption isotherm is the standard equation for determining specific area from gas adsorption data. The BET analysis was conducted using an Accusorb 2100E Physical Adsorption Analyzer (Micromeritics Instrument Corp.).

The specific surface areas of the CorWa and the CorWIPP sample are estimated to be 35.9 and 44.6 m^2/g, respectively.

2.2 Zeta Potential Measurement CorWIPP Sample

Electrokinetic measurements can be of considerable use in studying the chemical characteristics of hydrous mineral surfaces. It is customary to interpret electrokinetic data in terms

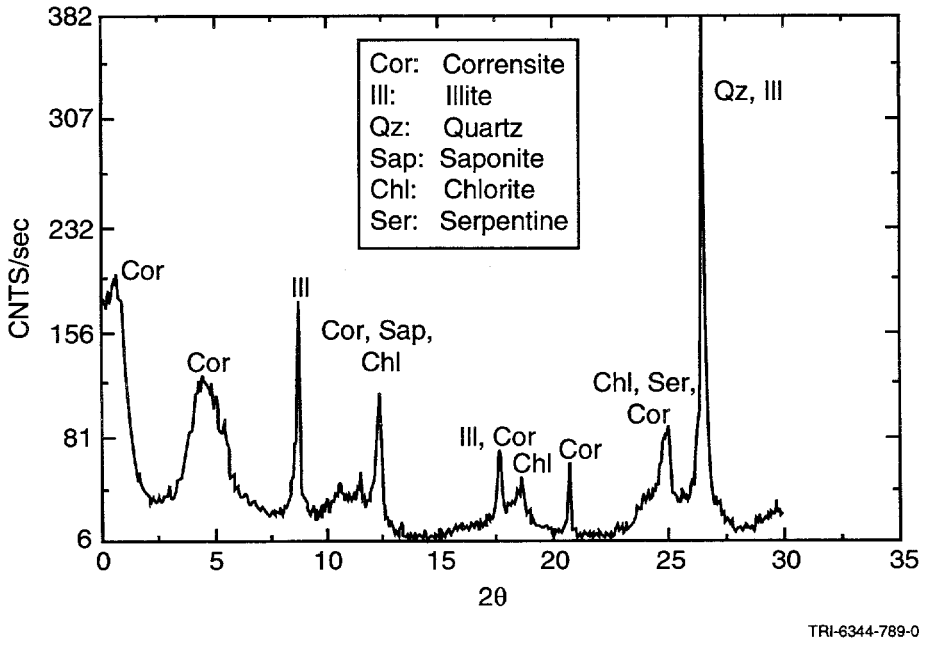

Figure 2-1. XRD pattern of disaggregated corrensite sample obtained from the WIPP Site (CorWIPP).

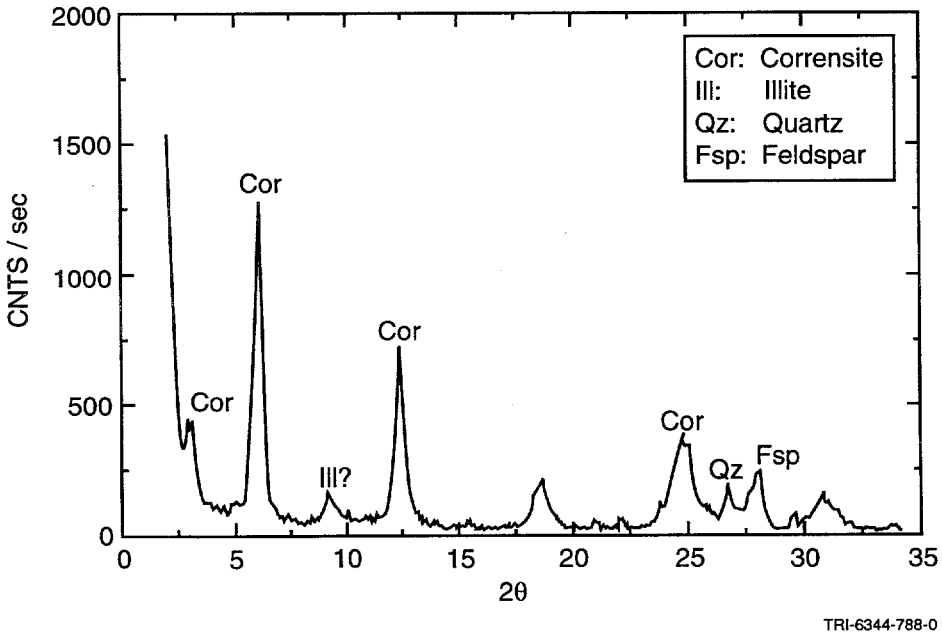

Figure 2-2. XRD pattern of the standard corrensite sample obtained from the Clay Mineral Society Source Clay Repository (CorWa).

of electrophoretic mobility or zeta potential. Zeta potential measurements have been extensively used as a technique to identify the amphoteric behavior of mineral surface hydroxyl groups. Zeta potential measurements of the corrensite samples were made using a Zeta Meter, Laser Zee Model 501. This instrument allows estimation of the potential at the shear plane of the particle surface by determining the rate of movement of the particles in a known electrical field.

Zeta potential measurements were made as follows. The desired volume of CorWIPP suspension was added to degassed deionized water in a 500 mL beaker (total suspension volume of 400 mL). Dry sodium perchlorate salt was then added to obtain the desired ionic strength ($\sim 5 \times 10^{-3}$ M). The particle velocities were measured at known pH values. The pH was then adjusted with 0.1 M $HClO_4$ or 0.1 M NaOH to cover a range from 4 to 10 in approximately 0.5 pH unit increments.

2.3 Titration of CORWIPP Sample

Potentiometric titrations were performed in 400 mL Griffin Teflon beakers maintained at 25°C using a Lauda Super K-2/R circulating water bath. A Teflon-coated magnetic stir bar was used to mix the suspension. An inert argon atmosphere kept carbon dioxide from entering the capped Teflon reaction vessel. The desired volume of CorWIPP suspension was added to degassed deionized water in the reaction vessel (total suspension volume of 100 mL). Sodium perchlorate was used to achieve ionic strengths of 0.001, 0.01, and 0.1 M. An Orion EA940 Ionalyzer and an Orion ROSS combination glass membrane pH electrode were used (millivolt response specification is 0.002 mV.) The potentiometric titration was then performed by first titrating with acid, then base, and finally adding acid again. The experiments were repeated on the same suspension at increasing ionic strengths by adding dry salt and repeating the above procedure to obtain a family of titration curves. An autotitrator was used which utilized 2.000-mL high-precision Gilmont syringes. The autotitrator monitored response time for equilibration after each addition of acid or base until a stable pH value (< 0.002 mV/min) was obtained.

2.4 Studies of U(VI) Loss to Container Walls and Choice of Bottles

Loss of U(VI) to container walls was observed. The reproducibility of uranyl analysis by stripping voltammetry was affected by adsorption on the container walls, where the loss was a function of pH. Uranyl solutions (4.2×10^{-7} M) in 0.1 M $NaClO_4$ as the electrolyte media were

prepared in several glass tubes and tubes of various polymer materials over the pH range 3 to 10. After 15 hr of shaking, the concentration of the uranyl in solution was measured. Tables in Appendix C show the loss of uranyl due to sorption onto the various container materials. Among others, polycarbonate tubes were observed to be nearly adsorption-free and were chosen for use. The maximum fraction of U(VI) lost due to adsorption on polycarbonate test tubes was 8% or less under the same conditions used for the U(VI) adsorption experiments.

2.5. Protocol of Adsorption Experiments

Batch equilibrium adsorption experiments were conducted in a parametric study to evaluate the characteristics of U(VI) interaction with the corrensite surface. All containers were soaked in 30% nitric acid for at least four hr and rinsed thoroughly in distilled water with a final rinse made in ultra pure deionized water from a Milli-Q system. The desired volume of CorWIPP suspension was added to degassed deionized water in approximately 25 50-mL Nalgene bottles (polycarbonate). Constant ionic strength, 0.05, was obtained by adding the required amount of $NaClO_4$ stock solution. The pH of the solution was adjusted by adding 0.01-0.1 M $HClO_4$ or 0.01-0.1 M NaOH via micropipettes to cover pH 4 to 10. After the pH of the suspension stabilized, the desired amount of uranyl stock solution was added. For experiments in which the effect of other ligands was to be studied, the desired quantities of ligand stock solution were added after the pH stabilized. Blank samples without CorWIPP also were prepared for each experiment. The total volume of the suspension was 45 mL and the total volume of acid or base added never exceeded 0.45 mL. The bottles then were shaken for approximately 15 hr. At shaking, the final or equilibrium pH was measured and recorded. The solid and solution phases were separated by centrifugation at 3,000 rpm for 30 mins. The residual concentrations of the U(VI) in solution were analyzed by Differential Pulse Cathodic Stripping Voltammetry (DPCSV) as described in Appendix D. The analytical conditions are shown in Table 2-1.

Table 2-1. Experimental Conditions for U(VI) Analysis by the DPCSV Method

Potential Scan Rate	10 mV/sec
Potential Scan Direction	–
Potential Scan Range	0.75 V
Initial Potential	-0.3 V
Modulation Amplitude	50
Display Direction	+
Output Offset Dial	0
Output Offset Toggle Switch	Off
Low Pass Filter	Off
Current Range	0.5 mA
Operating Mode	DP

3.0 RESULTS

3.1 Effects of pH on Uranyl Adsorption

The effect of pH on uranyl adsorption at room temperature (24°C) was studied by conducting batch adsorption experiments. Figure 3-1 shows the percent of U(VI) adsorbed onto the CorWIPP as a function of pH at different surface loadings. The amount of U(VI) adsorbed increases abruptly as pH increases over the pH range 4 to 6 and decreases in the high pH region. The percent of U(VI) adsorption increases with decreasing surface loading (ratio of the total U(VI) concentration to the adsorbent).

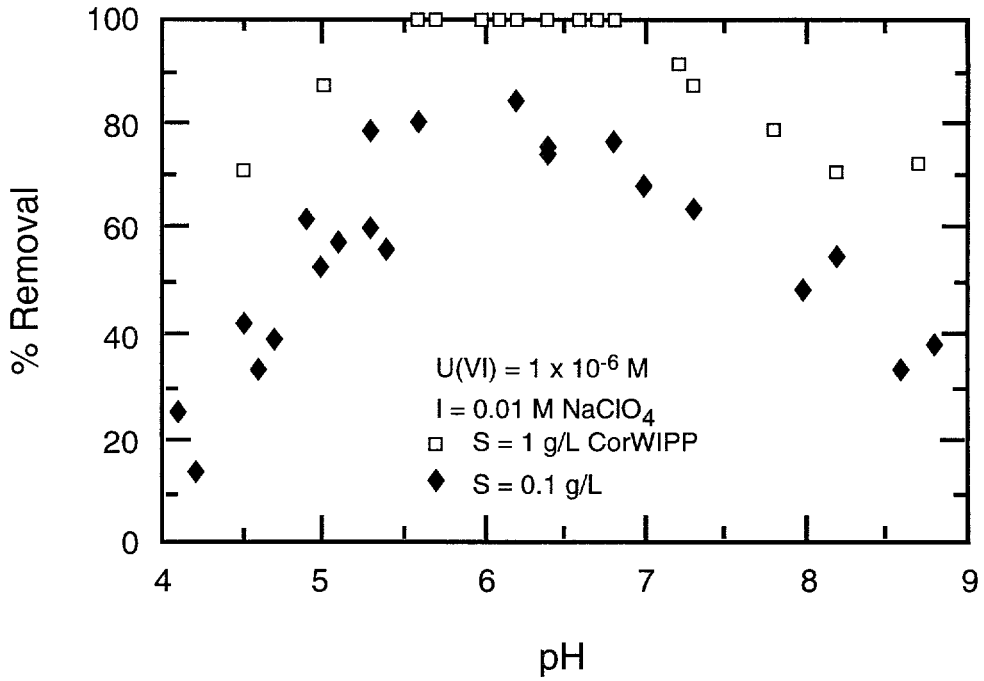

Figure 3-1 Data for U(VI) adsorption on corrensite at two solid/solution ratios at equilibrium (Final) pH.

3.2 Effect of Carbonate on Uranyl Adsorption

Figure 3-2 demonstrates that at pH ≥ 6, the adsorption of U(VI) in the air-saturated water is much less than that in the nitrogen-saturated (CO_2-free) water. Many researchers have reported that U(VI) adsorption is inhibited by the presence of carbonate species. To further examine this

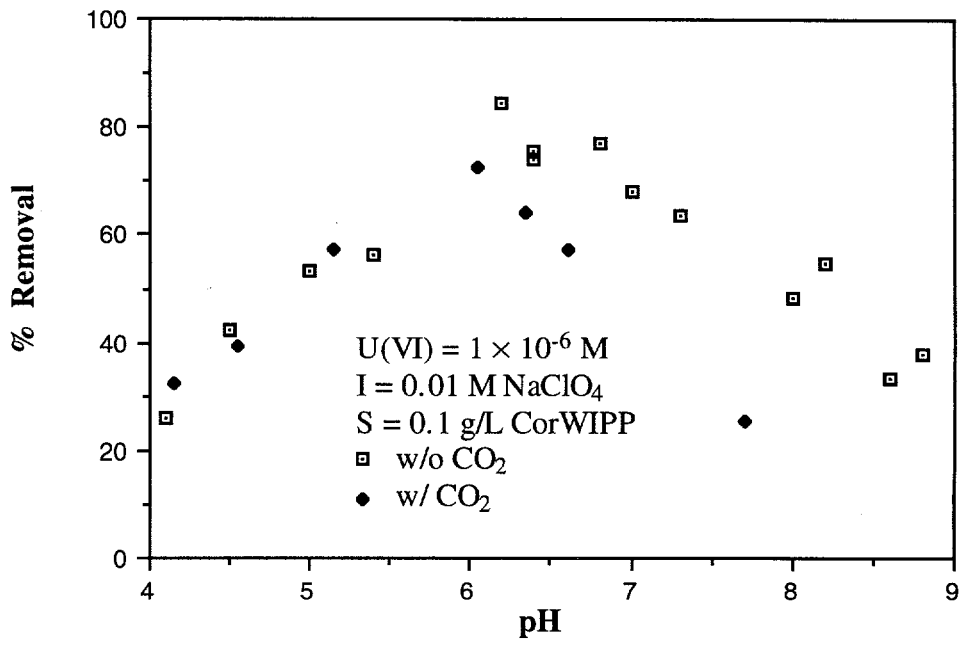

Figure 3-2. The effect of CO_2 (open system) on the adsorption of U(VI) by corrensite.

effect, $NaHCO_3$ salt was added to the suspension to bring the total carbonate concentration to the range 10^{-5} to 10^{-3} M. Other conditions were as previously described. As shown in Figure 3-3, U(VI) adsorption was significantly inhibited by the presence of carbonate at pH > 5. Also, the adsorption inhibition was proportional to the total carbonate concentration. It is proposed that the formation of carbonate uranyl complexes inhibits U(VI) adsorption.

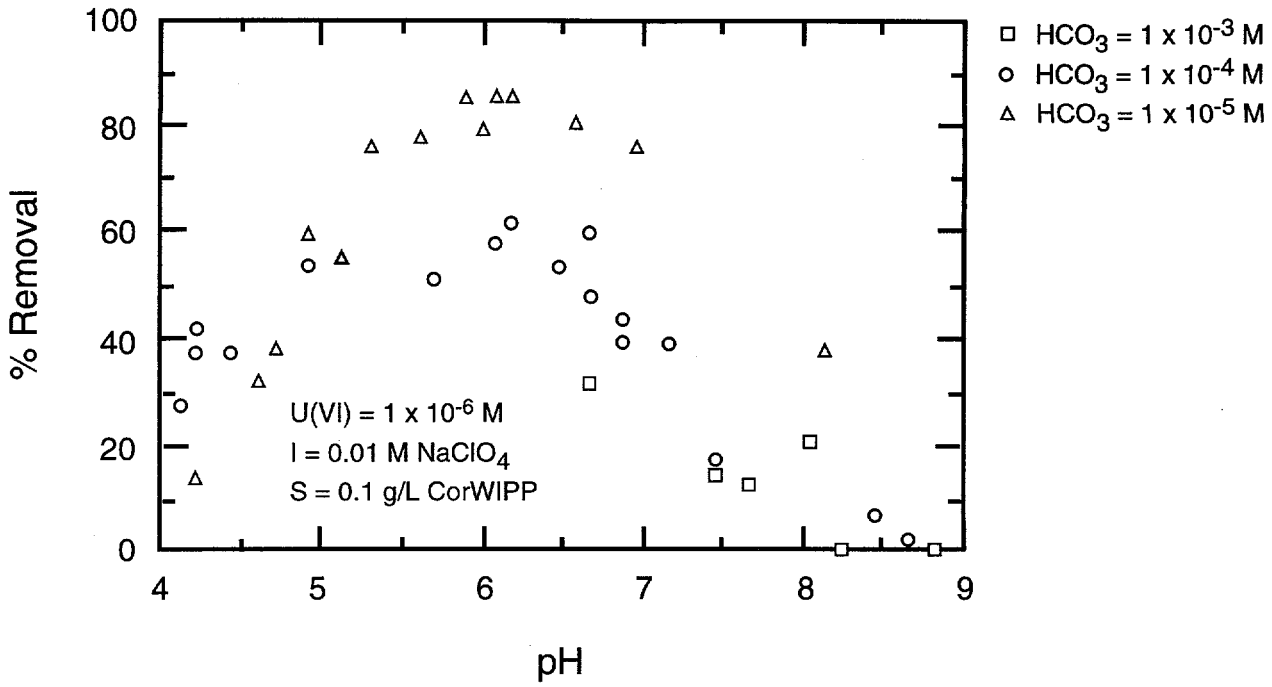

Figure 3-3. Data for U(VI) adsorption as affected by carbonate in closed systems.

3.3 Effect of Inorganic Cations on Uranyl Adsorption

Ca^{2+} and Mg^{2+} are among the most abundant cations in ground waters. Their typical concentration in natural ground water ranges from 10^{-2} to 10^{-4} M. Their effect on U(VI) adsorption was studied by adding calcium or magnesium perchlorate salts to the suspension to bring the total concentration to ~10^{-2} to ~10^{-4} M. Considering that the corrensite has a high Cation Exchange Capacity (CEC) (43-85 meq/100g), results as shown in Figures 3-4 and 3-5 indicate that Ca and Mg at the concentration ranges studied do not affect U(VI) adsorption. This suggests that Ca and Mg do not compete effectively with U(VI) at the sites at which U(VI) adsorption occurs. It can be inferred that these cations most likely undergo an ion exchange reaction with the Na^{+} at the basal plane sites.

3.4 Effect of Organic Chelating Agents on Uranyl Adsorption

Complex formation with organic ligands plays a significant role in determining the composition of pore water in the subsurface. Metal-organic interactions in natural waters are poorly understood, but are likely to be important factors in controlling the transport of metals in subsurface waters. These organic substances associate with metals through complexation and

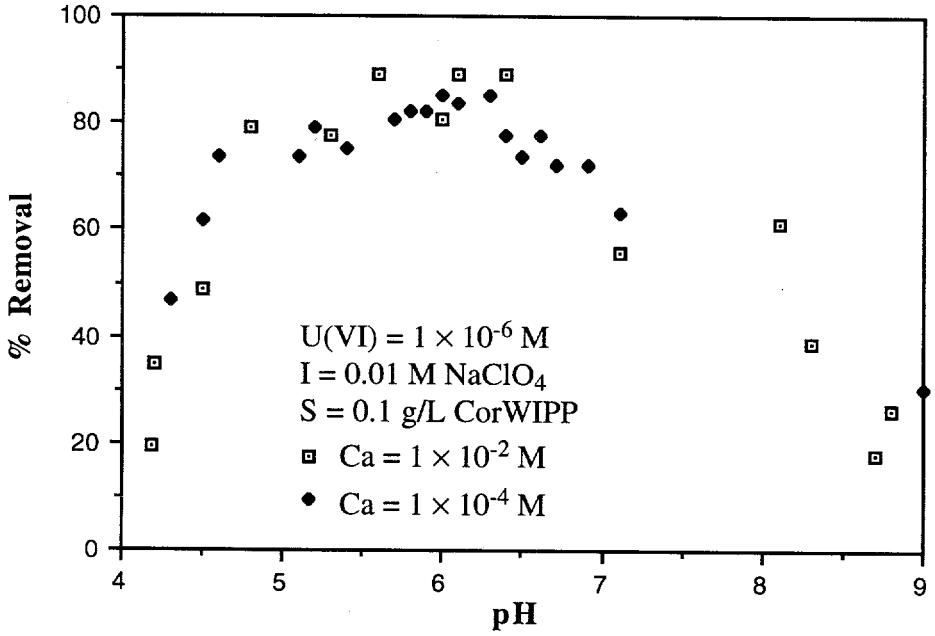

Figure 3-4. The effect of Ca^{2+} on the adsorption of U(VI) onto corrensite.

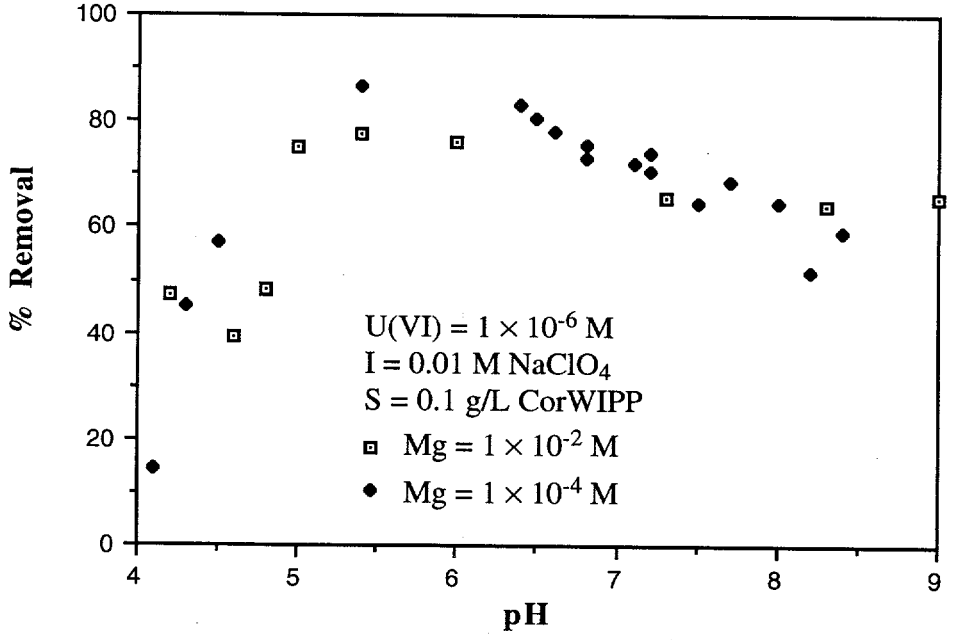

Figure 3-5. The effect of Mg^{2+} on the adsorption of U(VI) onto corrensite.

adsorption. An adsorbed organic film can mask the chemical properties of the underlying solid and create a surface whose chemical behavior is dominated by functional groups of adsorbed organic material. According to Benjamin and Leckie (1982) and Davis and Leckie (1978), the adsorption of a ligand may influence metal adsorption in the following ways:

- It may reduce the adsorption because of strong complex formation with the metal ions or by competing with the surface for available adsorption sites.
- It may not influence the adsorption because of weak complex formation ability with metal ions and lack of affinity for the surface.
- It may enhance the adsorption because of the strong complex formation with metal ions and also high affinity for the surface.

Among various organic complexing agents, ethylenediaminetetraacedtric acid (EDTA) and oxine were chosen for study for several reasons. Both EDTA and oxine are strong chelating agents for the uranyl ion. In addition, EDTA has often been used as a sequestering agent in the nuclear industry to clean up radionuclide spills and, hence, will likely be present in nuclear waste repository settings. To examine the effect of these organics on U(VI) adsorption, Na-forms of EDTA and oxine were added to the suspensions to give total EDTA or oxine concentrations of $\sim 10^{-5}$ to $\sim 10^{-6}$ M and similar adsorption experiments were repeated (Figures 3-6 and 3-7). Comparison of data in these figures with the corresponding figures for the ligand-free systems show that, under the experimental conditions, the presence of the organic complexing ligands inhibits the adsorption of U(VI). Because the effect of EDTA is more significant than that of oxine, it can be inferred that strong complex formation with U(VI) or competition with the surface for available adsorption sites may reduce the adsorption of U(VI).

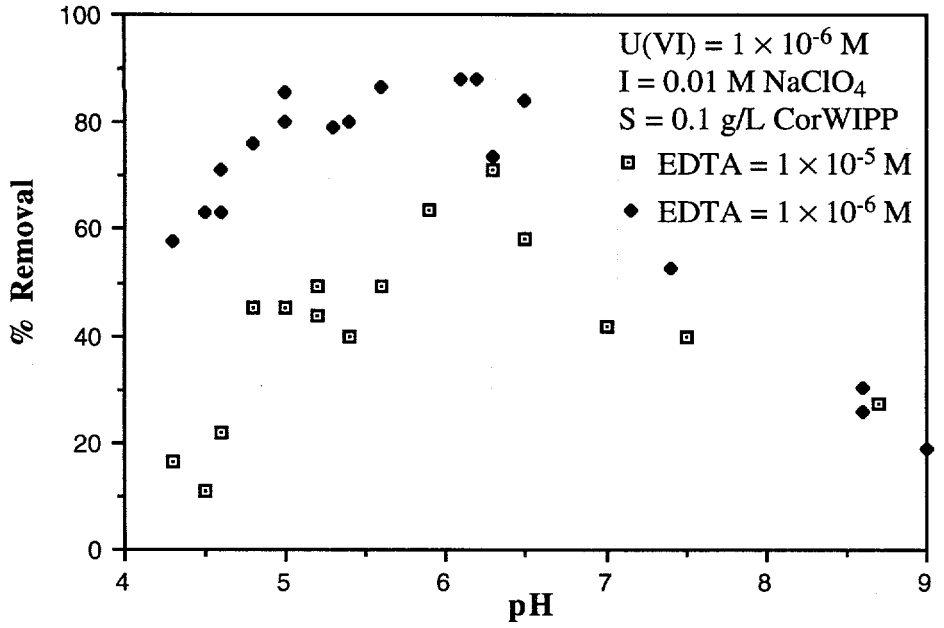

Figure 3-6. The effect of EDTA on the adsorption of U(VI) onto corrensite.

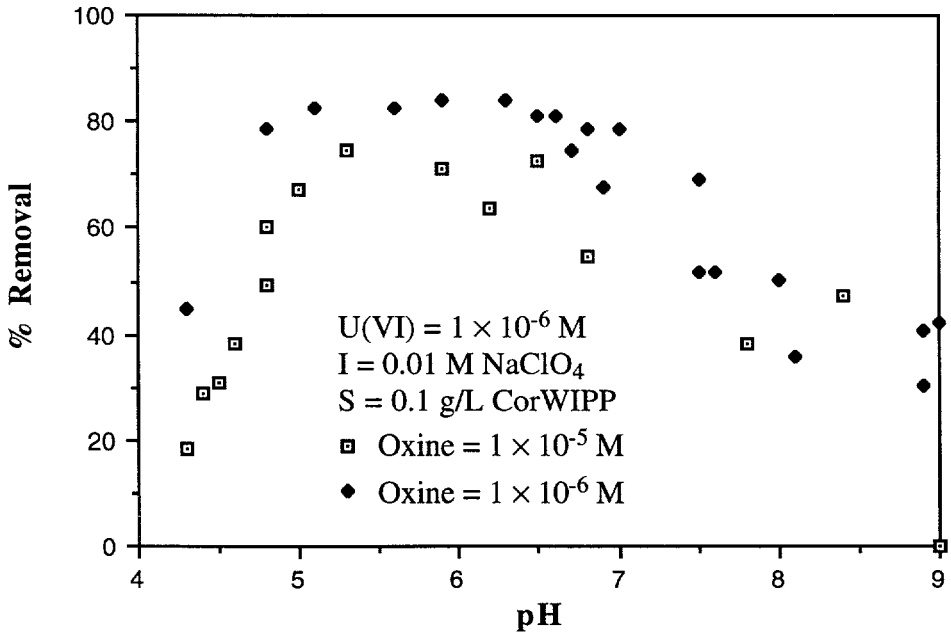

Figure 3-7. The effect of oxine on the adsorption of U(VI) onto corrensite.

3.5 Zeta Potential and Surface Charge Measurements

Clay minerals are composed of small plate-like particles ranging in diameter from a few hundredths of a micrometer to several micrometers and are electrically charged in the aquatic environment. Clays like corrensite carry a mixture of permanent charge and pH-dependent charge surfaces,

$$\sigma_o = \sigma_{oB} + \sigma_{oE} \qquad 3\text{-}1$$

where σ_o is the intrinsic surface charge; σ_{oB} is the surface charge at the basal plane (or the isomorphically substituted permanent structural surface charge), and σ_{oE} is the surface charge at the edge site (or the hydrolyzed surface charge). Depending on the site density of each kind of site, the overall surface charge will be different,

$$\sigma_o = \sigma_o f_E + \sigma_o f_B \qquad 3\text{-}2$$

where f represents the fraction of each surface area. The basal plane is characterized by its negative charge and lack of pH-dependent charge. On the other hand, the charge of edge sites is pH-dependent. It is known that the basal planes of clays, like corrensite, carry a much larger proportion of the permanently charged sites than edge sites. The zeta potential is the net potential at the shear plane beyond which supporting electrolytes electrostatically screen the resulting net surface charge. It can be expected that the overall zeta potential of the corrensite would reflect such a surface heterogeneity. Figure 3-8 presents the zeta potential of corrensite as a function of pH at two $NaClO_4$ concentrations. The data show that the surface potential of the corrensite is controlled by pH and the surface is negatively charged throughout the pH range studied. This qualitatively demonstrates the existence of both the permanently charged sites and the pH-dependent edge sites.

The pH-dependent charge can be further characterized by the acidic-alkalimetric titration method, because the amphoteric dissociation of the surface hydroxyl groups (surface protolysis) develops the surface charge residing in the hydroxylated layer. The titration technique has been the technique most frequently used for characterizing hydrous oxide minerals. Figure 3-9 shows the pH-dependent surface charge developed at the edge sites and measured by potentiometric titration. The Na^+ and ClO_4^- ions have no effect on the pH_{zpc} (zero point of charge) values, indicating these ions do not specifically form an inner-sphere complex with the surface hydroxyls (see Section 4.1). A pH_{zpc} value of 5.5 was estimated from the potentiometric titration data (Figure 3-9). The pH_{zpc} value was not observable from the zeta potential measurements (Figure 3-8). From the fact

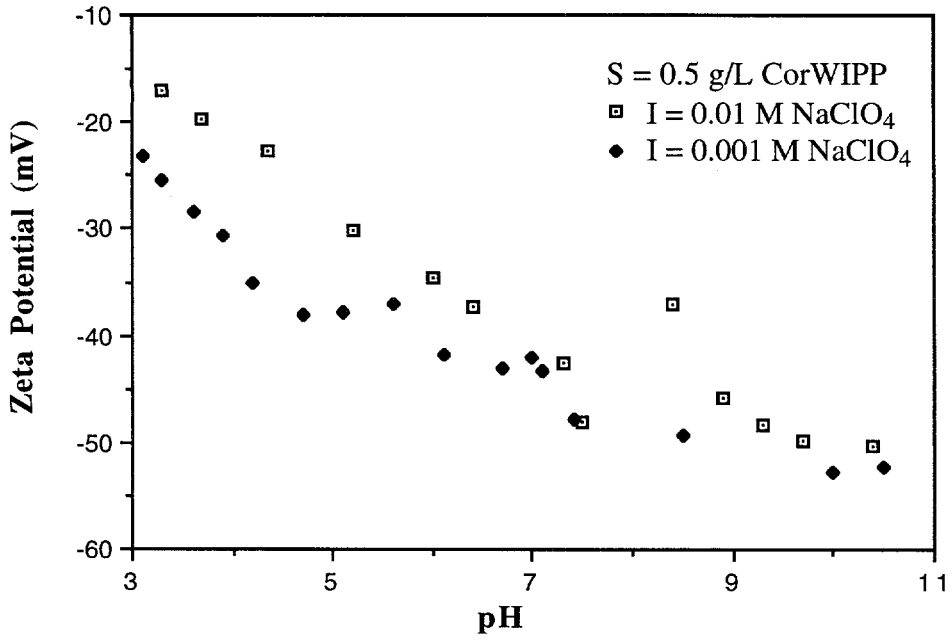

Figure 3-8. Zeta potential of corrensite in $NaClO_4$ electrolyte.

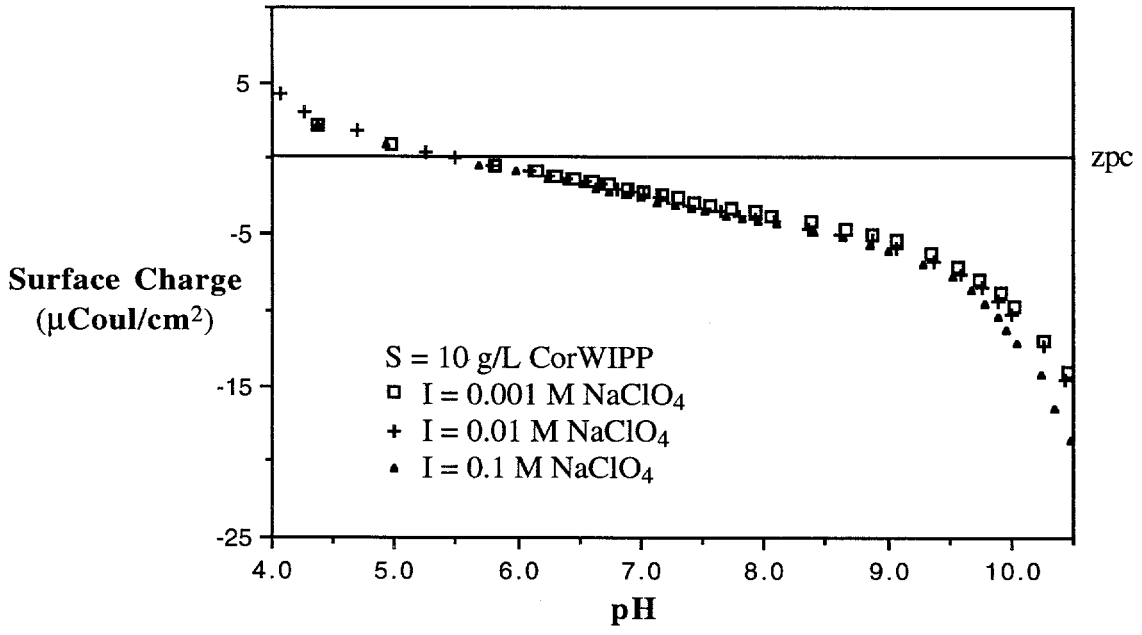

Figure 3-9. Surface charge of corrensite determined by acidic-alkalimetric titration.

that the edge sites are composed of two different entities such as SiOH and AlOH, it can be inferred that the edge sites behave like a composite oxide, a binary system of silica and alumina oxides. That is,

$$\sigma_{oE} = \sigma_{oE\text{-}Si} + \sigma_{oE\text{-}Al} \qquad 3\text{-}3$$

Considering the fact that silica oxide has a pH_{zpc} at pH ~1 to ~3 and alumina oxide at pH ~7 to ~9, the observed pH_{zpc} is consistent with the notion that the corrensite surface hydroxyls are composed of a mixture of SiOH- and AlOH-sites.

The pH-dependent adsorption behavior of U(VI) on the corrensite indicates that the adsorption occurs primarily at the edge sites. The inability of Ca and Mg to compete with U(VI) as shown in Figures 3-4 and 3-5 supports the notion of the edge-site adsorption of U(VI). Therefore, it is important to further characterize the surface properties of the edge sites to be used for modeling.

4.0 MODELING AND DISCUSSION

4.1 Models for Interactions at the Solid/Solution Interface

Surface complexation models (SCMs) are representations of reactions in the solid/solution interphase region based on direct analogy with solution chemical concepts. Interactions between solutes and the mineral surface are written as stoichiometric mass action equilibria using all the formalism of solution coordination chemistry. The only apparent difference from solution chemistry is the need to incorporate formal representation of the electric field effects of the charged surface. This section provides a brief overview of several of the SCMs considered for use in this work. More detailed discussions of the SCMs are found in Appendix A and references cited therein.

The SCMs consider the mineral surface hydroxyls as the active adsorption sites. When a surface hydroxyl functional group reacts with ions in the aqueous phase to form a stable unit, surface coordination is said to exist and the formation reaction is termed surface complexation. Two broad categories of surface complexes can be distinguished on structural grounds. If no molecule of water is interposed between the surface functional groups and adsorbate ions, the complex formed is called an inner-sphere complex; if at least one water molecule is interposed between the functional group and the bound adsorbate, the complex formed is called an outer-sphere complex. As a general rule, outer-sphere surface complexes involve predominantly electrostatic bonding mechanisms and therefore are less stable than inner-sphere surface complexes, which necessarily involve either ionic or covalent bonding or some combination of the two. The adsorption of counter ions at the inner Helmholtz plane is often governed by intrinsic stability constants and the electric potential. The diffuse layer is generally described by the Gouy-Chapman theory (Adamson, 1990).

The surface charge and the distribution of the counter ions are called the electrical double layer (EDL). Depending upon the interpretation of the EDL structure, there are several versions of the SCMs, three of which are presented here: the Diffuse Layer Model (DLM), the Constant Capacitance Model (CCM), and the Triple Layer Model (TLM). These models differ in the conceptual description of the EDL used as the basis of adsorption modeling. A more detailed discussion of the three SCMs is given in Appendix A.

The DLM employs the Gouy-Chapman theory in the (outer) diffuse layer, but assumes that there is no potential drop between the (inner) Stern layer and the diffuse layer. Although the DLM

is insensitive to ionic strength changes over the wide range of ionic strength conditions typically encountered, the simplicity of the model makes it an attractive alternative to the other two SCMs. The CCM assumes that the capacitance does not change in the Stern layer and the specific chemical adsorption becomes the major source of energy on the surface. The CCM requires one more fitting parameter than the DLM does. Its advantage over the DLM is a better capability to fit titration data at a single ionic strength. The TLM assumes two constant capacitances and one diffuse layer. The best feature of the TLM is that it specifically accounts for background electrolyte effects by assuming ion-pair complexes between the surface sites and electrolytes.

The ion-exchange model describes the adsorption and desorption of bound and dissolved ions at fixed charge sites. In this model, all adsorbed ions are located at the surface plane and the surface electrical potential is ignored. The exchange processes are reversible and described by the law of mass action involving the concentrations of aqueous ions and bound species.

The two-site model is a modified double-layer model that is used to describe the adsorption behavior of clay minerals. As discussed in Appendix A, clay minerals have two types of surface charge: fixed (negative) charge sites that are found on the basal plane of clays and edge sites with pH-dependent charge. The ions adsorbed by the basal sites are assumed to be either specifically adsorbed or located in the diffuse layer. Adsorption of ions by the basal sites is not significantly affected by pH; the surface charge and potentials are determined by the charge due to isomorphic substitution. The pH-dependent edge sites are modeled with the TLM-SCM as discussed in Appendix A.

4.2 Chemical Characteristics of the Corrensite Surface: Estimation of TLM Parameters

Interpretation of surface chemical reaction data requires an accurate knowledge of the experimental system components, including the acidities of surface functional groups, solution speciation and the electrostatic status of the mineral surface. The techniques used to obtain this information are described below. More detailed descriptions are found in Kent et al. (1986) and in the references cited therein.

4.2.1 Determination of Total Site Concentration (N_S)

An estimate of the total protolyzable site concentration, N_s, is needed to estimate SCM parameters. Several methods have been used to evaluate the concentration of the surface hydroxyl sites. In this study, a single extrapolation method was adopted. Since this method ignores the specific adsorption of the electrolytes, it is inapplicable to a wide range of electrolyte concentrations, particularly at high ionic strength. However, this approach has its own merit; it is simple, has reasonable accuracy, and can be conducted with the titration data without separate experimental settings. At $pH > pH_{zpc}$, the total surface site concentration in an inert electrolyte can be approximated as:

$$N_s = B[\{SOH\} + \{SO^-\}] \qquad 4\text{-}1$$

$$\sigma_{O^-} = B\{SO^-\} \qquad 4\text{-}2$$

where $B=10^6F/S_e$; F is the Faraday constant (96,490 coul/mol); S_e is the edge site surface area (m^2/L) in the suspension, and the units of N_s and σ_{O^-} are the same.

Substituting Equations 4-1 and 4-2 into Equation A-4 (see Appendix A), yields

$$\{H^+\} = N_s K_{a2}^{int}/\sigma_{O^-} - K_{a2}^{int} \qquad 4\text{-}3$$

A plot of $\{H^+\}$ versus $1/\sigma_{O^-}$ yields a slope and intercept allowing determination of N_s (2.6×10^{-6} moles sites/nm^2) (Figure 4-1), where { } indicates surface activity. Comparison to the CEC value of the corrensite, 43-85 meq/100g (9.5 to 19.5×10^{-6} moles sites/nm^2), suggests that approximately 12 to 22% of the total sites are pH-dependent edge sites.

4.2.2 Double Extrapolation Technique to Determine Surface Ionization Constants

The single extrapolation method assumed sufficiently low ionic strengths such that the surface site complexation can be ignored. The double extrapolation method improves upon this assumption. James et al. (1978) and James and Parks (1982) determined the surface ionization and complexation constants from potentiometric titration data by this method. That is, Equation A-4 can be rearranged and combined with Equation A-6 to give

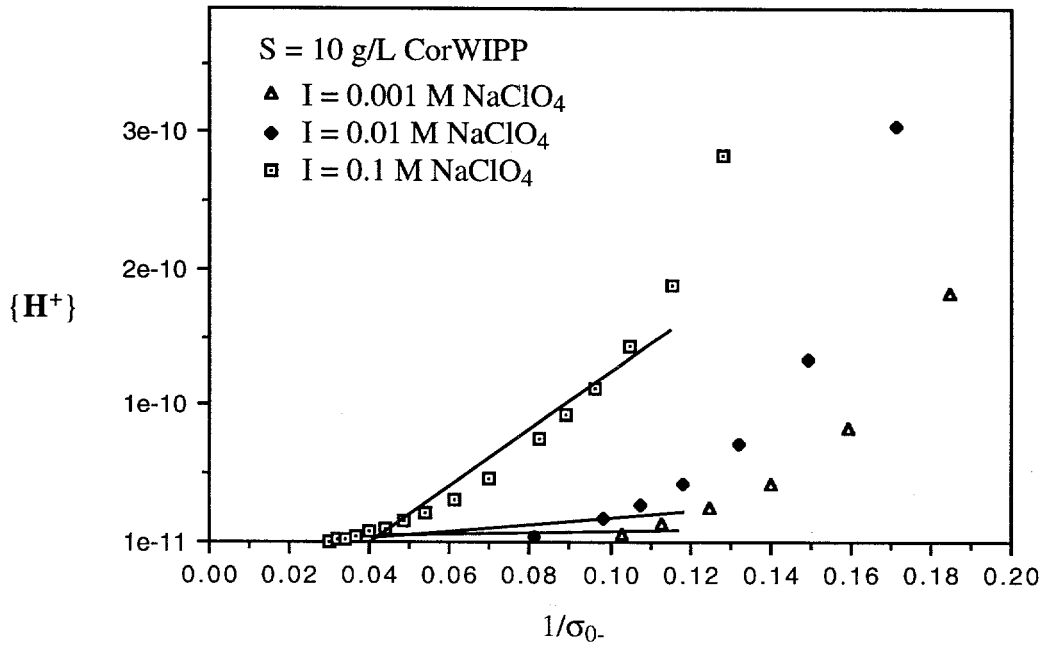

Figure 4-1. A plot of $\{H^+\}$ vs $1/\sigma_{O-}$.

$$K_{a2}^{int} = \frac{\alpha_-}{1 - \alpha_-}[H^+]\exp\left(-\frac{e\Psi o}{kT}\right) \qquad 4\text{-}4$$

where $\alpha_-=\sigma_{o-}/N_s$. N_s can be estimated by Equation 4-3. In negative logarithmic form,

$$pK_{a2}^{int} = pH - \log\frac{\alpha_-}{1 - \alpha_-} + \frac{e\Psi o}{2.3kT}$$

$$= pQ_{a2}^{int} + \frac{e\Psi o}{2.3kT} \qquad 4\text{-}5$$

The apparent acidity quotient, pQ_{a2}^{int}, can be determined at different ionic strengths and plotted as a function of $\alpha_- + (C_{NaClO_4})^{1/2}$. The double extrapolation is obtained as follows. First, the pQ_{a2} values for each ionic strength are extrapolated to $\alpha_- = 0$. Second, the double extrapolated point at $\alpha_- = C = 0$ gives pK_{a2}^{int}. The method of determination is illustrated in Figure 4-2, where the determined pK_{a2}^{int} value is 7.3. With a similar process, after rearranging Equation A-3, the first ionization constant, pK_{a1}^{int}, also can be determined.

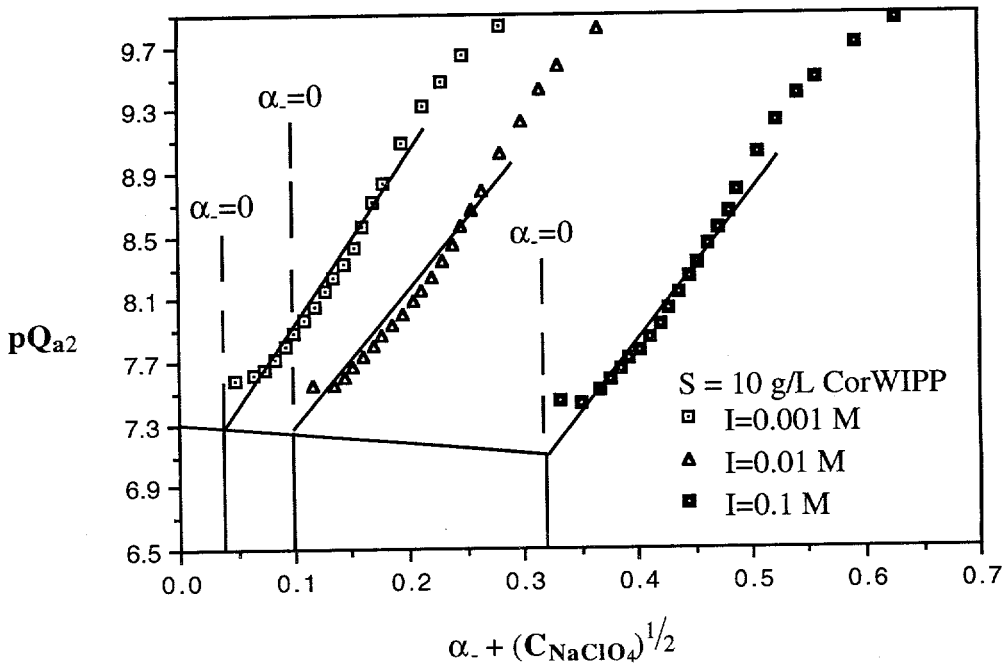

Figure 4-2. A plot of pQ_{a2} vs $\alpha_- + (C_{NaClO_4})^{1/2}$.

In this study, the titration experiments were conducted in the pH range 4 to 10 because dissolution of the corrensite may occur beyond this pH range. Near the pH_{zpc}, the amounts of {SO-} and $\{SOH_2^+\}$ groups are comparable and therefore the pQ_{a1}^{int} and pQ_{a2}^{int} calculated from the titration data near the pH_{zpc} are inaccurate. Thus, the pK_{a1}^{int} was not determined by this method. As an alternate, the pK_{a1}^{int} can be determined from the following equation, provided the value of the second ionization constant, as well as pH_{zpc} are known,

$$pH_{zpc} = (pK_{a1}^{int} + pK_{a2}^{int})/2 \qquad 4\text{-}6$$

The value $pK_{a1}^{int} = 3.7$ was obtained in this manner.

To account for the specific adsorption of the electrolytes, Davis et al. (1978) proposed the formation of ion pairs at charged surface sites. For adsorption of electrolyte ions,

$$SOH + Na_s^+ = SO^- - Na^+ + H_s^+ : K_{Na}^{int} \qquad 4\text{-}7$$

The mass action expression for the stoichiometry in Equation 4-7 is

$$[SO^- - Na^+] = \frac{[SOH][Na^+]}{[H^+]} \exp\left[\left(e\Psi_o - e\Psi_\beta\right)/kT\right] K_{Na}^{int} \qquad 4\text{-}8$$

which leads to

$$pK_{Na}^{int} = pH - \log\frac{\alpha_-}{1-\alpha_-} + \log[Na^+] + \left(e\Psi_o - e\Psi_\beta\right)/2.3kT$$

$$= pQ_{Na} + \left(e\Psi_o - e\Psi_\beta\right)/2.3kT \qquad 4\text{-}9$$

A plot of pQ_{Na} vs (α_- - log [Na+]) can be used to determine pK_{Na}^{int}. The double extrapolated point at α_- = log C = 0 gives pK_{Na}^{int} = 6.5 (Figure 4-3). No extrapolation technique was applied to estimate $pK_{ClO_4^-}$ because of the large inherent error. The value used for $pK_{ClO_4^-}$ was arrived at by adjusting the value for data at 0.1 g/L CorWIPP (Figure 3-1) and was maintained constant for other modeling efforts. The effect of $pK_{ClO_4^-}$ is essentially negligible except at pH < 5.

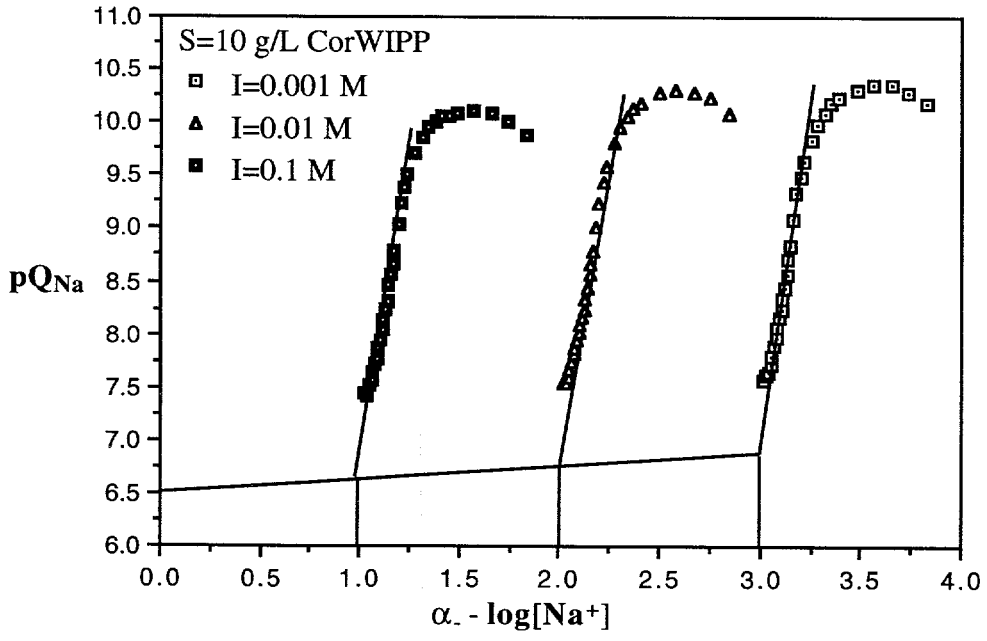

Figure 4-3. A plot of $pQNa^{int}$ vs. (α_- - log [Na+]).

5.0 SUMMARY AND CONCLUSIONS

5.1 Summary of Experimental and Model Results

Radionuclide/clay interactions may be an important mechanism of radionuclide retardation in ground-water systems. The amount of radionuclide sorption within the Culebra at the WIPP Site will be strongly dependent on the solution chemistry and the nature of the minerals exposed to the solutions. Collecting experimental data that can be used to predict the degree of uranium sorption over a wide range of solution compositions is a prerequisite to performance assessment calculations.

In applying the SCMs for adsorption modeling, it is necessary to determine the chemical properties of the adsorbent and adsorbate. Most SCM studies have been conducted with well characterized laboratory-made pure solids, rather than with naturally occurring ones, such as corrensite, the dominant clay mineral occurring in the Culebra Dolomite at the WIPP Site. Various attempts were made in this report to extract the information regarding the corrensite surface characteristics needed for the adsorption modeling. Partitioning of uranyl ions between aqueous solution and the corrensite surface will be modeled by the triple layer surface complexation model in future studies.

Characteristic properties of clay minerals are large specific surface area, the ability to react chemically under low temperature conditions, large CEC, and high surface charge. The fine particles of the corrensite sample disaggregated by the ultrasonic processor were used for the physicochemical surface characterization and batch adsorption experiments. The X-ray diffractogram of the clay showed a corrensite pattern. The specific surface area of the corrensite sample was determined by the BET method to be 44.6 m^2/g. A cation exchange capacity of 85 meg/100g for the CorWIPP reference was determined using the sodium acetate exchange method and a CEC of 31 meq/100g using the Mg-Ca exchange method.

The clay surface is divided into two major regions: the basal planes and the plate edges. These two regions are thought to differ in surface chemical and adsorption properties. Zeta potential measurements and titration experiments of the corrensite sample qualitatively describe the surface charge characteristics of the corrensite, showing that the surface is composed of a mixture of permanent charge at the basal plane and net pH-dependent charge of -SiOH and -AlOH sites at the edge of the corrensite surface.

Corrensite is an effective adsorbent for U(VI) in dilute solutions under mildly acidic conditions. The pH-dependent adsorption behavior of U(VI) onto corrensite indicates that adsorption occurs at the edge sites. The amount of U(VI) adsorbed onto corrensite increases abruptly as the pH increases over the range 4 to 6 and decreases at higher pH (> 7.5). The amount of U(VI) sorption increases with decreased surface loading.

Table 5-1 summarizes measurements of U(VI) adsorption by various clay minerals at neutral pH (Ames et al., 1983). These results indicate that other phyllosilicates are effective adsorbents for U(VI) under conditions similar to those examined in this report. The pH dependence of uranium adsorption has also been examined by Hsi and Langmuir (1985). These researchers investigated the adsorption behavior of U(VI) onto four different Fe oxyhydroxides and observed that there was no decrease of U(VI) adsorption at high pH values for amorphous $Fe(OH)_3$, goethite, and synthetic hematite, but that adsorption by natural hematite decreased at high pH.

Table 5-1. Experimental Mean Values for Sorption of Uranium by Secondary Minerals at 25°C from 0.01 M NaCl Solutions*

Solid	Initial U(VI) (mole/liter)	Equilibrium U(VI) (mole/liter)	U(VI) on solid (mole/g)
Illite 1.438×10^{-6}	1.044×10^{-5} 2.954×10^{-8}	2.601×10^{-7} 1.548×10^{-8}	1.119×10^{-7}
Kaolinite 1.438×10^{-6}	1.044×10^{-5} 3.034×10^{-8}	2.522×10^{-7} 1.573×10^{-8}	1.139×10^{-7}
Montmorillonite 1.438×10^{-6}	1.044×10^{-5} 2.981×10^{-8}	1.852×10^{-7} 1.584×10^{-8}	1.153×10^{-7}
Nontronite 1.438×10^{-6}	1.044×10^{-5} 4.734×10^{-8}	1.255×10^{-6} 1.538×10^{-8}	1.016×10^{-7}
Silica gel 1.438×10^{-6}	1.044×10^{-5} 2.981×10^{-8}	2.345×10^{-7} 1.549×10^{-8}	1.123×10^{-7}

*Ames et al. (1983).

The inability of Ca^{2+} and Mg^{2+} (10^{-2} M) to compete with U(VI) is consistent with edge-site adsorption for U(VI). Therefore, in future studies, speciation models will consider the surface hydroxyls at the edge sites as the adsorption sites. TLM parameters determined by the double extrapolation technique will be used for chemical speciation calculations including adsorption simulation with the computer program, HYDRAQL.

The effects of chemical species that frequently occur in the ground water and nuclear waste and may influence U(VI) adsorption were examined. It was found that carbonate complexation inhibits U(VI) adsorption and only the carbonate-free species adsorb. Ca and Mg at the concentration ranges studied (10^{-2} to 10^{-4} M) do not affect U(VI) adsorption. Complex formation with organic ligands plays a significant role in determining the composition of pore water in the subsurface. These organic ligands associate with metals through complexation and adsorption reactions. The presence of organic complexing ligands inhibits the adsorption of U(VI). Because the effect of EDTA is more significant than that of oxine, it can be inferred that strong complex formation with U(VI) or competition with the surface for available adsorption sites may reduce the adsorption of U(VI) or remobilize adsorbed U(VI).

5.2 Conclusions and Recommendations

The K_d approach, used in transport codes to calculate the partitioning of radioelements between ground water and surrounding solids, is not appropriate for all aspects of radionuclide migration because K_d, rather than being constant, is directly linked to solution composition and solid properties. The K_d value is an empirical parameter that is a function of a number of variables, including radionuclide concentration, oxidation potential, ionic strength, pH, composition of the sorbing surface and solution, and time. As an alternative to the K_d approach and a more conceptually satisfying approach, the SCMs, incorporating various solution and surface chemical characteristics, have been studied for radionuclide partitioning in geochemical settings. This modeling approach has its merits in the inherent flexibility of the models in simulating a wide range of chemical scenarios.

Modeling adsorption data with TLM-SCM requires a serious evaluation of the quality of the experimental data and a data set that extends over a broad range of suspension conditions. The process of model fitting to a data set provides a structured means of evaluating the quality and quantity of the data. The methodologies for collecting and modeling adsorption data and defining

constraints on simulations with verified models are bound together in the SCM approach. Several steps are involved in applying the SCM approach to describing adsorption. The adsorption properties of the substrate must be characterized. The best available thermodynamic data for the formation of solution complexes involving the adsorbate must be collected and corrected to the appropriate standards and reference states. Adsorption studies must be carried out over the widest possible range of suspension conditions. Stoichiometries and binding constants for surface complexes that give the best fit to the experimental data over the range of suspension compositions studied must be determined.

The corrensite from the WIPP Site is an effective adsorbent for U(VI). In the ligand-free system, adsorption of U(VI) on corrensite occurs between ca. pH 4 and 10, which is within the pH range of ground water. Since ground water contains various solution compositions, studies were continued to investigate the adsorption behavior of U(VI) in the presence of those species (such as Ca^{2+}, Mg^{2+}, and organic ligands), which might frequently be found in ground water, especially at the nuclear waste disposal sites. In the range of concentrations studied, there is no significant effect of Ca^{2+} and Mg^{2+} on the adsorption of U(VI) onto the corrensite. However, it is possible that those cations at higher concentrations might reduce the adsorption of U(VI). Further studies should be made to predict the extent of the effect of those cations.

Despite the decisive role played by adsorption in determining the fate of many metals and the ubiquity of soluble organic ligands, the effect of organic ligand-metal complex formation on the adsorption characteristics of metal ions is not entirely understood. It is known that there are three possible outcomes: inhibiting, no effect, or enhancement. In this study, it was found that EDTA and oxine inhibit the adsorption of U(VI). It thus can be inferred that strong complex formation with U(VI) or competition with the surface for available adsorption sites may reduce the adsorption of U(VI). This information reveals the significance of the role of organic ligands in the transport of uranium. However, it is not yet known how and to what extent those organic ligands will affect the movement of uranium in subsurface waters. To further understand the role of organic ligands on the transport of uranium, several possible factors should be considered. These are the structure of metal-ligand complex, the pH-dependent species of metal-ligand complex, and individual adsorption characteristics including their individual binding constants.

6.0 REFERENCES

Adamson, A.W. 1990. *Physical Chemistry of Surfaces*. 5th ed. New York, NY: John Wiley & Sons, Inc.

Ames, L.L., J.E. McGarrah, and B.A. Walker. 1983. "Sorption of Trace Constituents from Aqueous Solutions onto Secondary Minerals. I. Uranium," *Clays and Clay Minerals*. Vol. 31, no. 5, 321-334.

Benjamin, M.M., and J.O. Leckie. 1982. "Effects of Complexation by Cl, SO_4, and S_2O_3 on the Adsorption Behavior of Cadmium on Oxide Surfaces," *Environmental Science and Technology*. Vol. 16, no. 3, 162-170.

Cranwell, R.M., et al. 1987. *Risk Methodology for Geologic Disposal of Radioactive Waste: Final Report*. SAND81-2573, NUREG/CR-2452. Albuquerque, NM: Sandia National Laboratories.

Daniels, W.R., et al. 1982. *Summary Report on the Geochemistry of Yucca Mountain and Environs*. LA-9328-MS. Los Alamos, NM: Los Alamos National Laboratory.

Davis, J.A., and J.O. Leckie. 1978. "Effect of Adsorbed Complexing Ligands on Trace Metal Uptake by Hydrons Oxides," *Environmental Science and Technology*, Vol. 12, no. 12, 1309-1315.

Davis, J.A., R.O. James, and J.O. Leckie. 1978. "Surface Ionization and Complexation at the Oxide/Water Interface. 1. Computation of Electrical Double Layer Properties in Simple Electrolytes," *Journal of Colloid and Interface Science*. Vol. 63, no. 3, 480-499.

De Regge, P., P. Henrion, M. Monsecour, M. Put, M.P. Cremers, and A. Maes. 1988. "Facts and Features of Radionuclide Migration in Boom Clay," *Radioactive Waste Management and the Nuclear Fuel Cycle*. Vol. 10, nos. 1-3, 1-20.

Delegard, C.H., and G.S. Barney. 1983. *Effects of Hanford High-Level Waste Components on Sorption of Cobalt, Strontium, Neptunium, Plutonium and Americium on Hanford Sediments*. RHO-RE-ST-1-P. Richland, WA: Rockwell International Corporation.

Franz, J.A., L.Y. Martin, and D.J. Wiggins. 1982. *Behavior of Reduced Technetium-99 and Its Organic Complexes on Hanford Soil*. PNL-4178. Columbus, OH: Battelle Columbus Labs.

Gregg, S.J., and K.S.W. Sing. 1982. *Adsorption, Surface Area and Porosity*. London: Academic Press.

Grim, R.E. 1968. *Clay Mineralogy*. 2nd ed. New York, NY: McGraw-Hill.

Hayes, K.F., G. Redden, W. Ela, and J.O. Leckie. 1990. *Application of Surface Complexation Models for Radionuclide Adsorption*. NUREG/CR-5547, PNL-7239. Richland, WA: Pacific Northwest Laboratories.

Hsi, C.D., and D. Langmuir. 1985. "Adsorption of Uranyl onto Ferric Oxyhydroxides: Application of the Surface Complexation Site-Binding Model," *Geochimica et Cosmochimica Acta*. Vol. 49, no. 9, 1931-1941.

Huang, C.P., and W. Stumm. 1973. "Specific Adsorption of Cations on Hydrous γ - Al_2O_3," *Journal of Colloid and Interface Science*. Vol. 43, no. 2, 409-420.

James, R.O., and G.A. Parks. 1982. "Characterization of Aqueous Colloids by Their Electrical Double-Layer and Intrinsic Surface Chemical Properties," *Surface and Colloid Science*. Ed. E. Matijevic. Vol. 12, 119-216.

James, R.O., J.A. Davis, and J.O. Leckie. 1978. "Computer Simulation of the Conductimetric and Potentiometric Titrations of the Surface Groups on Ionizable Latexes," *Journal of Colloid and Interface Science*. Vol. 65, no. 2, 331-344.

Jones, B.F., and A.H. Weir. 1983. "Clay Minerals of Lake Abert, an Alkaline, Saline Lake," *Clays and Clay Minerals*. Vol. 31, no. 3, 161-172.

Kent, D.B., V.S. Tripathi, N.B. Ball, and J.O. Leckie. 1986. *Surface-Complexation Modeling of Radionuclide Adsorption in Sub-Surface Environments*. Technical Report No. 294. Stanford, CA: Stanford University, Department of Civil Engineering.

Krumhansl, J.L., K.M. Kimball, and C.L. Stein. 1990. *A Review of WIPP Repository Clays and Their Relationship to Clays of Adjacent Strata*. SAND90-0549. Albuquerque, NM: Sandia National Laboratories.

Lappin, A.R., R.L. Hunter, D.P. Garber, and P.B. Davies, eds. 1989. *Systems Analysis, Long-Term Radionuclide Transport and Dose Assessments, Waste Isolation Pilot Plant (WIPP), Southeastern New Mexico; March 1989*. SAND89-0462. Albuquerque, NM: Sandia National Laboratories.

Leckie, J.O., and V.S. Tripathi. 1985. "Effect of Geochemical Parameters on the Distribution Coefficient K_d," *Heavy Metals in the Environment, Proceedings of the Fifth International Conference, Athens, September 1985*. Ed. T.D. Lekkas. Edinburgh: CEP Consultants. Vol. 2, 369-371.

Marietta, M.G., S.G. Bertram-Howery, D.R. Anderson, K.F. Brinster, R.V. Guzowski, H. Iuzzolino, and R.P. Rechard. 1989. *Performance Assessment Methodology Demonstration: Methodology Development for Evaluating Compliance with EPA 40 CFR 191, Subpart B, for the Waste Isolation Pilot Plant*. SAND89-2027. Albuquerque, NM: Sandia National Laboratories.

Papelis, L., K.F. Hayes, and J.O. Leckie. 1988. *HYDRAQL: Program for the Computation of Chemical Equilibrium Composition of Aqueous Batch Systems Including Surface-Complexation Modeling of Ion Adsorption at the Oxide/Solution Interface*. Technical Report TECE-48086. Stanford, CA: Stanford University, Department of Civil Engineering.

Park, S.W., and C.P. Huang. 1989. "The Adsorption Characteristics of Some Heavy Metal Ions onto Hydrous CdS(s) Surface," *Journal of Colloid and Interface Science*. Vol. 128, no. 1, 245-257.

Popeliak, R.S., R.L. Beauheim, S.R. Black, W.E. Coons, C.T. Ellingson, and R.L. Olsen. 1983. *Brine Reservoirs in the Castile Formation, Waste Isolation Pilot Plant (WIPP) Project, Southeastern New Mexico.* TME-3153. Albuquerque, NM: D'Appolonia Consulting Engineers.

Rancon, D., and J. Rochon. 1980. "Retention of Long-Life Radionuclides by Diverse Argillaceous Minerals," *The Use of Argillaceous Materials for the Isolation of Radioactive Waste, Proceedings of the Workshop, Paris, September 10-12, 1979.* Paris: Nuclear Energy Agency, Organisation for Economic Co-Operation and Development. 139-146.

Sanchez, A.L., W.R. Schell, and T.H. Sibley. 1982. "Distribution Coefficients for Plutonium and Americium on Particulates in Aquatic Environments," *Environmental Migration of Long-Lived Radionuclides, Proceedings of an International Symposium, Knoxville, TN, July 27-31, 1981.* STI/PUB/597. Vienna: International Atomic Energy Agency. 188-203.

Sargent, F.P., and T.T. Vandergraaf. 1988. "Radionuclide Migration R&D in the Canadian Nuclear Fuel Waste Management Program," *Radioactive Waste Management and the Nuclear Fuel Cycle.* Vol. 10, no. 1-3, 21-40.

Schindler, P.W., B. Fürst, R. Dick, and P.U. Wolf. 1976. "Ligand Properties of Surface Silanol Groups. I. Surface Complex Formation with Fe^{3+}, Cu^{2+}, and Pb^{2+}," *Journal of Colloid and Interface Science.* Vol. 55, no. 2, 469-475.

Sewards, T. 1991. *Characterization of Fracture Surfaces in Dolomite Rock, Culebra Dolomite Member, Rustler Formation.* SAND90-7019. Albuquerque, NM: Sandia National Laboratories.

Sewards, T., M.L. Williams, K. Keil, S.J. Lambert, and C.L. Stein. 1991. "Mineralogy of the Culebra Dolomite," *Hydrogeochemical Studies of the Rustler Formation and Related Rocks in the Waste Isolation Pilot Plant Area, Southeastern New Mexico.* Eds. M.D. Siegel, S.J. Lambert, and K.L. Robinson. SAND88-0196. Albuquerque, NM: Sandia National Laboratories. 3-1 through 3-4.

Sewards, T., A. Brearley, R. Glenn, I.D.R. MacKinnon, and M.D. Siegel, 1992. *Nature and Genesis of Clay Minerals of the Rustler Formation in the Vicinity of the Waste Isolation Pilot Plant in Southeastern New Mexico.* SAND90-2569. Albuquerque, NM: Sandia National Laboratories.

Sholkovitz, E.R. 1983. "The Geochemistry of Plutonium in Fresh and Marine Water Environments," *Earth-Science Reviews.* Vol. 19, no. 2, 95-161.

Siegel, M.D. 1990. "A Model for the Chemical Evolution of Groundwater in the Culebra Dolomite," *Abstracts with Programs, Geological Society of America.* SAND90-1763A. Vol. 22, no. 7, A101.

Siegel, M.D., K.L. Robinson, and J. Myers. 1991. "Solute Relationships in Groundwaters from the Culebra Dolomite and Related Rocks in the Waste Isolation Pilot Plant Area, Southeastern New Mexico," *Hydrogeochemical Studies of the Rustler Formation and Related Rocks in the Waste Isolation Pilot Plant Area, Southeastern New Mexico.*

Eds. M.D. Siegel, S.J. Lambert, and K.L. Robinson. SAND88-0196. Albuquerque, NM: Sandia National Laboratories. 2-1 through 2-164.

Sposito, G. 1984. *The Surface Chemistry of Soils*. New York, NY: Oxford University Press.

Till, J.E., and H.R. Meyer, eds. 1983. *Radiological Assessment*. NUREG/CR-3332, ORNL-5968. Oak Ridge, TN: Oak Ridge National Laboratory for U.S. Nuclear Regulatory Commission.

Tripathi, V.S. 1983. "Uranium (VI) Transport Modeling: Geochemical Data and Submodels." Ph.D. Dissertation. Stanford, CA: Stanford University, Department of Civil Engineering.

Uematsu, K. 1988. "Japanese Approaches to the Assessment of Radionuclide Migration in the Geosphere," *Radioactive Waste Management and the Nuclear Fuel Cycle*. Vol. 10, no. 1-3, 145-158.

Van Olphen, H. 1977. *An Introduction to Clay Colloid Chemistry*. 2nd ed. New York, NY: Wiley-Interscience.

ACRONYMS

AEM	Analytical Electron Microscopy
AIS	Air Intake Shaft
BET	Brunauer, Emmett, and Teller (method)
CCM	Constant Capacitance Model
CPB	Cetyl Pyridinium Bromide
CEC	Cation Exchange Capacity
CorWa	Standard Corrensite from State of Washington, obtained from Clay Mineral Society Source Clay Repository
CorWIPP	Corrensite Sample from WIPP Site
DLM	Diffuse Layer Model
DPCSV	Differential Pulse Cathodic Stripping Voltammetry
EDL	Electrical Double Layer
EDS	Energy Dispersive Analysis
EDTA	Ethylenediaminetetraacedtric Acid
EGME	Ethylene Glycol Monoethyl Ether
PDI	Potential Determining Ion
SCM	Surface Complexation Model
SNL	Sandia National Laboratories
TEM	Transmission Electron Microscopy
TLM	Triple Layer Model
TDS	Total Dissolved Solid
TRU	Transuranic
WIPP	Waste Isolation Pilot Plant
XRD	X-Ray Diffraction

SYMBOLS

-AlOH	Aluminol hydrolyzed surface site
B	Conversion factor from moles per liter to microcoulombs per square centimeter
C_i	Concentration of species i in mol/L
C_1, C_2	Inner layer and outer layer capacitances ($\mu F/cm^2$)
e	Fundamental charge
F	Faraday constant (96,490 coulombs/mole)
I	Ionic strength (mol/L)
K	Thermodynamic constant
K_d	Distribution coefficient (mL/g)
K_i^{int}	Intrinsic stability constant of species i
k	Boltzmann constant
N_s	Density of adsorption site ($\mu mol/m^2$, site/nm^2, or $\mu coul/cm^2$)
pH_{zpc}	pH at zero point of charge
pQ	Quantity in double extrapolation procedure
S	Solid concentration (g/L)
S_A	Specific surface area (m^2/g)
-SiOH	Silica hydrolyzed surface site
SOH	Hydrolyzed surface site
α_+, α_-	Fraction of surface sites that are positively or negatively charged
β	β-layer: compact part of electrical double layer
$\sigma_o, \sigma_\beta, \sigma_d$	Charge densities at surface (o-plane), β-plane, and in diffuse layer, respectively, in $\mu coul/cm^2$
$\psi_o, \psi_\beta, \psi_d$	Electrical potential at surface (o-plane), β-plane, and in diffuse layer, respectively, in volts

{i}	Surface concentration of species i in mol/L or surface activity in mol/L
[i]	Aqueous concentration of species i in mol/L

APPENDIX A:
MODELS FOR ADSORPTION ON LAYERED SILICATES (CLAYS)

APPENDIX A:
MODELS FOR ADSORPTION ON LAYERED SILICATES (CLAYS)

A.1 Generation of Surface Charge

Clay minerals are small hydrous layer silicates and are part of the phyllosilicate family. The layer silicates are constructed of planes of atoms forming tetrahedral and octahedral sheets arranged in various combinations (Bailey, 1980). The tetrahedral cations are primarily Si and Al, and rarely Fe. The octahedral sheet consists of cations (Al, Fe, Mg) that are octahedrally coordinated by shared apical oxygens plus unshared hydroxyls that lie at the center of the hexagonal hole formed by the basal oxygens. The combination of one tetrahedral sheet and one octahedral sheet is called a 1:1 layer. The unshared plane of anions in the octahedral sheet consists of hydroxyls. A 2:1 layer consists of an octahedral sheet sandwiched between two tetrahedral sheets. Where the tetrahedral cations are all Si and the octahedral cations all Al (dioctahedral) or all Mg (trioctahedral), the layers are electrostatically neutral (pyrophyllite and talc) and held together by Van der Waals bonds. Most hydrous layer silicates have some isomorphic substitution of lower charged cations for higher charged cations. This produces a negative charge that is neutralized by positively charged ions between the layers (interlayer material). Interlayer materials can be individual cations (micas), hydrated cations (expanded clays), hydroxide groups (chloritics), and hydroxide octahedral sheets (chlorite). The latter combination, chlorite, is referred to as a 2:2 or 2:1:1 structural unit. The 1:1, 2:1 and 2:2 layers can occur interstratified in various combinations to produce a wide variety of interstratified or mixed-layer minerals.

Interstratified or mixed-layer minerals are constructed of two different layer types arranged on a fine scale in a regular or irregular pattern. In principle, the layer structures of all these minerals are similar enough that interstratification of any combination of minerals could be envisaged. Corrensite was originally defined as a regular 1:1 interstratification of trioctahedral (Mg) chlorite and "swelling chlorite" (Lippmann, 1954). The term is now generally applied to regularly stratified 1:1 chlorite/smectite phyllosilicates. Corrensite is a relatively common phyllosilicate and forms under a wide variety of conditions. Corrensite is particularly common in evaporite rocks (marls, dolomite, anhydrite, and halite).

Characteristic properties of clay minerals are large specific surface area, the ability to react chemically under low temperature conditions, large cation exchange capacity (CEC), and high surface charge. Although the chemical compositions of clay minerals are remarkably similar, the

above characteristics of each clay mineral can vary considerably (Table A.1). The heterogeneous distribution at surface clay minerals with variable high surface charges makes the adsorption of radionuclides in subsurface environments quite complex. It is therefore necessary to discuss briefly the origin of surface charge on clay minerals.

The clay surface can be divided into two major regions: the basal planes and the edges. These two regions are thought to differ in surface chemical and adsorption properties (Sposito, 1984). Adsorption sites at the edges result primarily from charge produced by the abrupt ending of the structure. These edge sites often are referred to as "broken bonds." The edges of clay minerals contain ions not fully coordinated, much the same as oxide surfaces. These edges also adsorb H^+ and OH^- to form hydroxylated surfaces, which in turn develop a surface charge through amphoteric association or dissociation, i.e., the broken bonds act as weak acids and/or weak bases. Thus, the edge charge is pH dependent, becoming more negative with increasing pH. The edges typically contain a mixture of silanol and aluminol sites, the density of which depends on the degree of hydration and the relative proportions of octahedral and tetrahedral sheets.

The charge on the basal plane, on the other hand, is thought to result from isomorphic substitution within the clay structure. Charge location and density is a function of clay type. The most commonly acknowledged source of surface charge on clay particles is from the structural imperfection in the basal-plane surfaces of clay minerals. Structural imperfections, due to ion substitution or site vacancies, frequently result in permanent charge on the clay surface. In theory, this charge may assume either a positive or negative value. However, due to ion size limitation, a lower valence element will generally substitute for one with a higher valency (Singh and Uehara, 1986). For example, Al^{3+} substituting for tetrahedral Si^{4+} leads to a deficiency of positive charge on the crystal lattice. The resulting charge is negative on the clay structure, resulting in a permanent surface charge.

A.2 Surface Complexation Models

Surface complexation models (SCMs) are used to compute the extent of adsorption over a wide range of solution composition. SCMs capture the essential chemical nature of the adsorption process; consequently, they are incorporated readily into schemes for computing equilibrium states of aqueous systems. The surface reactivity of the solid phase is, in essence, a cooperative property and derives from the chemical behavior of surface functional groups. A surface functional group is

Table A-1. Cation Exchange Capacity and Surface Area of Some Charged Components*

Mineral Group	CEC mmol/kg	Surface Area (m^2/g) N_2	EGME	Other	Method
Phyllosilicates					
Kaolinite	2—150	6—42(8.5)†	5—30	12—17	H_2O
				8—25	Negative ads
				9—32	CPB
				20—21	Dodecylamine HC1
				17—18.7	Orthophenanthroline
				8.6—32	Methylene blue
Metahalloysite	50—100	40—50	10—102		
Halloysite	400—500	10—30	10—430		
Smectites	570—2000	12—158	309—859	40—215	CO_2
Montmorillonite		144†	693†	138—527	H_2O
				295—743	Methylene blue
				300—308	Dodecylamine HCI
				564—778	Orthophenanthroline
				800	CPB
Vermiculite	1000—2100	0.5—431	50—800	31—70	CO_2
				76.9	Orthophenanthroline
				84	n-butane
				100—300	H_2O
				726	CPB
Illite	100—400	43—195	65—139	52—86	H_2O
				72—162	CO_2
				96—209	CPB
				118—127	Orthophenanthroline
				78	Methylene blue
Allophane	500—1500	145—300	247—549	0	CPB
				435—534	H_2O
				68—251	Titration
Pyrophyllite	<10		2—3		
Muscovite	<10				
Biotite	<10				
Chlorite	100—400				
Corrensite		36(CorWa)†, 44.6 (CorWIPP)†			
Palygorskite	150—300	130—150	165		
Sepiolite	180—390			330	Hexane
				60	CPB
				268—296	CO_2
Zeolites	2290—5680				
Oxide hydroxide	20—40				
Gibbsite		0.385—7.51(11.2)†			
Geothite		(~48)†		14—177	H_2O
Boehmite		143			
Hematite		(~15)†		34—45	H_2O
Noncryst.		(~600)†		250	SO_4 ads
Ferrihydrite				295	H_2O
Noncryst. Al		111 (100-200)†			

*Sources: Sparks (1986)
†Data from this study.

a chemically reactive molecular unit bound into the structure of a solid at its periphery such that the reactive components of the units are in contact with solution. Therefore, to model ion-adsorption phenomena at the solid/water interface, it is essential to know the properties of the solid phase close to the interface.

Most solid particles in aquatic environments are electrically charged. This surface charge is one of the most important parameters governing the ion adsorption behavior. It is generally well known that the surface charge may be created in two different ways. Imperfections within the interior of the crystal lattice of the particle may be the cause of a net positive or negative lattice charge (as discussed in Section A.1) or the surface can be charged by adsorbing particular ionic solutes [potential determining ions (PDI)]. Adsorption of PDIs creates an electric charge at the solid surface; many studies have observed that H^+ and OH^- are PDIs for many of the naturally occurring oxides in the aqueous phase. Establishment of charge on such particles is viewed as a result of the chemisorption of water to form a hydroxylated surface.

The hydroxylated layer on the surface exhibits amphoteric behavior. The amphoteric dissociation of the surface hydroxide group (protolysis reaction) develops the surface charge residing at the hydroxylated layer. The protolysis reaction leads to either a positive or negative charge density, depending upon solution pH. The protolysis reactions of the surface hydroxyl groups are depicted as

$$SOH_2^+ = SOH + H^+ \qquad \text{A-1}$$

$$SOH = SO^- + H^+; \qquad \text{A-2}$$

where SOH_2^+, SOH and SO^- stand for the positive, neutral, and negative surface hydroxyl functional sites, respectively.

In the interphase region, the surface charge and the distribution of the counter ions are defined as the electrical double layer (EDL). Depending on the interpretation of the EDL structure, there are several versions of the SCMs, three of which are presented here: the Diffuse Layer Model (DLM), the Constant Capacitance Model (CCM), and the Triple-Layer Model (TLM). Figure A.1 gives a schematic picture of these models. These models differ in the conceptual description of the EDL used as the basis of adsorption modeling. A more detailed discussion of the three SCMs is given in the following sections.

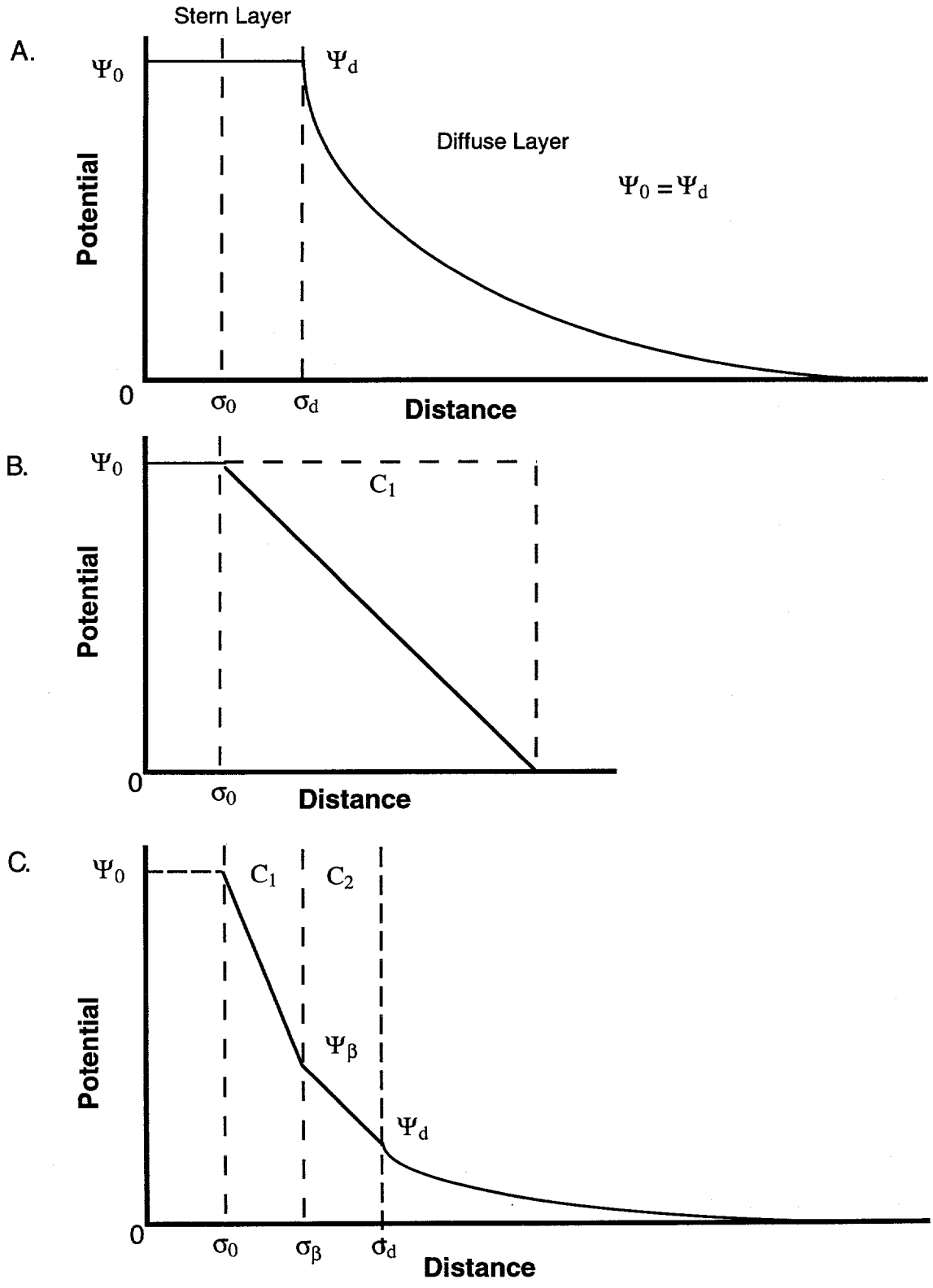

Figure A-1. Structure of surface complexation models at the solid/solution interface: A. Diffuse Layer Model, B. Constant Capacitance Model, C. Triple-Layer Model.

A.2.1 Diffuse Layer Model

The DLM treats the hydrous surface as being composed of amphoteric hydroxyl groups, which are capable of undergoing reactions analogous to acids and bases in aqueous solution (Healy et al., 1977; Westall and Hohl, 1980; Huang, 1981; James and Parks, 1982; Dzombak and Morel, 1986; Hayes et al., 1987). In the DLM, the surface/water interface is considered to comprise two layers of charge: a surface (Stern) layer and a diffuse layer of counter ions in solution. All specifically adsorbed ions are assigned to one surface layer and all nonspecifically adsorbed counter ions are assigned to the diffuse layer. A Gouy-Chapman (Adamson, 1990) distribution of ions is assumed for the solution side of the interface. The simple two-layer concept of the surface/water interface incorporated in the diffuse layer model is illustrated in Figure A.1A.

Surface ionization reactions are responsible for the amphoteric behavior of the solid surface as expressed by Equations A-1 and A-2. The corresponding mass law equations are

$$K_{a1}^{int} = \frac{\{SOH\}\{H^+\}}{\{SOH_2^+\}} \qquad \text{A-3}$$

$$K_{a2}^{int} = \frac{\{SO^-\}\{H^+\}}{\{SOH\}} \qquad \text{A-4}$$

where { } represents the surface activity of the species. The activity coefficients for the surface species are assumed to be equal to one. The total number of the surface active sites, N_s, is the sum of these three hydroxy groups:

$$N_s = \{SOH_2^+\} + \{SOH\} + \{SO^-\} \qquad \text{A-5}$$

The surface concentration of the proton $\{H^+\}$ is related to its bulk phase concentration, $[H^+]$, (where [ ] represents concentration) by the Boltzmann equation:

$$\{H^+\} = [H^+] \exp \frac{-e\Psi_o}{kT} \qquad \text{A-6}$$

where e, Ψ_o, k and T are the units of electronic charge, surface potential, Boltzmann constant, and absolute temperature, respectively. The DLM assumes that there is no potential drop in the Stern layer, i.e., $\Psi_o = \Psi_d$. The surface charge σ_o is related to the potential at the surface ψ_o by

$$\Psi_o = \frac{2kT}{ze} \sinh^{-1} \frac{\pi}{2kT\varepsilon I} \sigma_o \qquad \text{A-7}$$

where z is the charge of the symmetrical electrolyte and ε is the dielectric constant. The surface charge can be determined by acidic-alkalimetric titration. The DLM, as the simplest SCM, has only three adjustable parameters: the two surface ionization constants, K_{a1}^{int} and K_{a2}^{int}, and total number of surface sites, N_s. The DLM accounts for the effect of changing background electrolyte concentration on surface protolysis reactions. Several research groups have applied this model to the adsorption modeling.

A.2.2 Constant Capacitance Model

The CCM is based on the assumption that surface hydroxyl groups form only inner-sphere surface complexes with adsorbed species (Hohl and Stumm, 1976; Dzombak and Morel, 1986; Hayes et al., 1987). In the CCM, the surface complexation reactions involve only H^+ and OH^-. The CCM is restricted to modeling experimental data obtained at one ionic strength. The relationship between surface charge and surface potential thus becomes linear (Figure A.1B):

$$\sigma_o = C_1 \Psi_o \qquad \text{A-8}$$

where C_1 is the capacitance. According to this model, the specific chemical adsorption becomes the major source of energy on the surface. Compared to the DLM, the CCM has one more model parameter, the capacitance, C_1.

A.2.3 Triple Layer Model

Yates et al. (1974) proposed the site-binding model in which PDI and bulk electrolyte ions form interfacial ion pairs with a discretely charged surface based on Levine's (1971) model. According to this model (Figure A.1C), the potential drop across each layer can be expressed as,

$$\Psi_o - \Psi_\beta = \sigma_o / C_1 \qquad \text{A-9}$$

$$\Psi_\beta - \Psi_d = -\sigma_d / C_2 \qquad \text{A-10}$$

where C_1 and C_2 are integral capacitances of the respective regions of the compact part of the double layer. C_1 and C_2 are usually taken as 120-140 $\mu F/cm^2$ and 20 $\mu F/cm^2$, respectively, to fit most of the experimental surface charge data. Later, Davis and Leckie (1978) combined Yates' site-binding model with the surface-ionization and electrolyte-binding model of Davis et al. (1978).

The TLM incorporates an O-plane (or surface plane) with a fixed number of amphoteric groups; a β-plane (or inner Helmholtz plane) where counter ions are located; and a d-layer (or diffuse layer), which starts at the outer Helmholtz plane. The adsorption of counter ions at the inner Helmholtz plane is related to the number of charged surface groups. Thus, a positive counter ion will likely associate with a negatively charged surface group and a negative counter ion will likely associate with a positive surface group. If a single electrolyte NaCl is present, the possible interface species are: SOH, SOH_2^+, SO^-, $SOH_2^+Cl^-$, and SO^-Na^+. Along with surface ionization (Equations A-1 and A-2) , the electrolyte binding equilibria are as follows:

$$SO^- + Na^+ = SO^-Na^+ \qquad \text{A-11}$$

$$SOH_2^+ + Cl^- = SOH_2^+Cl^- \qquad \text{A-12}$$

With these equilibria, it is possible to relate the density of the interface species (electrolyte ion pairs at the charged surface sites) to the bulk phase concentrations of the components:

$$K_{Na+}^{int} = \frac{\{SO^-Na^+\}}{\{SO^-\}[Na^+]} \exp\left(e\Psi_\beta/kT\right) \qquad \text{A-13}$$

$$K_{Cl-}^{int} = \frac{\{SOH_2^+Cl^-\}}{\{SOH_2^+\}[Cl^-]} \exp\left(-e\Psi_\beta/kT\right) \qquad \text{A-14}$$

The concentrations of ions in the electrical double layer are expressed in terms of the Boltzmann distribution. The magnitude of the charge density in the surface plane, σ_o, and the inner Helmholtz plane, σ_β, are functions of the concentrations of the different interface-species:

$$\sigma_o = F\,[\{SOH_2^+\} + \{SOH_2^+Cl^-\} - \{SO^-\} - \{SO^-Na^+\}] \qquad \text{A-15}$$

$$\sigma_\beta = F\,[\{SO^-Na^+\} + \{SOH_2^+Cl^-\}] \qquad \text{A-16}$$

The total charge over the interface requires electroneutrality:

$$\sigma_o + \sigma_\beta + \sigma_d = 0 \qquad \text{A-17}$$

where σ_d is the diffuse layer charge, which is given by Equation A.7 and is obtained from the Gouy-Chapman equation for a symmetrical electrolyte. The total number of surface sites is determined experimentally and is given by:

$$N_s = \{SOH_2^+\} + \{SOH_2^+Cl^-\} + \{SOH\} + \{SO^-\} + \{SO^-Na^+\} \qquad \text{A-18}$$

The number of adsorption sites in the inner Helmholtz plane is not fixed in the triple-layer model. Therefore, once values for the parameters N_s, C_1, C_2, and K_i^{int} values have been selected, the

above equations are solved simultaneously to obtain the concentrations of surface and aqueous species.

A.3 Ion Exchange Model

The stoichiometric adsorption-desorption process of bound and dissolved ions at fixed charge sites is called ion exchange (Babcock, 1963; Gast and Klobe, 1971; Jardine and Sparks, 1984). The surface electric potential is completely ignored in this model; all adsorbed ions are located in the surface plane. Direction, extent, and velocity of an ion exchange process depend on the relative concentration and the properties of the involved ions. The exchange processes are reversible and can be described by the law of mass action. The intensity of the bond is different for the various bound ions and exchanging ions. The binding intensity increases with the valence state or within a single valence state with the atomic number and probably with the radius. The ion exchange processes involve the competing ions A^+ and B^+ and the cation exchanger R^-:

$$A^+ + B^+R^- = A^+R^- + B^+ \qquad \text{A-19}$$

and can be described by a selectivity coefficient, K_B^A:

$$K_B^A = \frac{[A^+R^-][B^+]}{[A^+][B^+R^-]} = \frac{[A^+R^-]/[A^+]}{[B^+R^-]/[B^+]} \qquad \text{A-20}$$

where $[A_+]$ and $[B_+]$ are the concentration of these ions in solution and $[A_+R_-]$ and $[B_+R_-]$ are the concentrations in the adsorbed phase.

The ion exchange reaction is a dominant adsorption mechanism in determining the distribution coefficient, K_d. The selectivity coefficient can be related to K_d if the total cation exchange capacity Q of the exchanger and the total competing cation concentration in solution C are known, and the system under consideration is at equilibrium:

$$K_B^A = K_d^A \frac{[C - (A^+)]}{[Q - (A^+R^-)]} \qquad \text{A-21}$$

If the contaminant A^+ is present in amounts much less than B^+, $[A^+]$ is much less than C, and if $[A^+R^-]$ is less than Q, the relationship can be simplified to

$$K_d^A = \frac{K_B^A Q}{C} \qquad \text{A-22}$$

Therefore, under these conditions K_d is directly proportional to the CEC and the selectivity coefficient and inversely proportional to the total competing cation concentration. Correlation between K_d and CEC of solids has been studied. A linear relationship between CECs and K_d for a wide range of rock types and minerals was observed, implying that CEC can be used as a representative measure in evaluating K_d of nuclides governed by ion exchange adsorption (Allard et al., 1980). However, it was also found that K_d is not a constant and is affected by several factors.

A.4 Two-Site Model

A two-site model applies the double-layer approach to adsorption modeling based on the origin and behavior of two types of surface charge (Kleijn, 1981). The SCMs do not include the permanent charge sites such as the fixed charge on the basal plane of clays. The two-site model, a modified triple-layer model, includes the basal fixed charge sites and the edge protolysable sites. In contrast to the edge sites, the basal-plane surfaces of clay minerals are only negatively charged due to isomorphic substitution. The H^+ and OH^- ions are not considered to be of major significance with regard to the charge on the basal-plane surfaces of the clay minerals. The counter ions, balancing the negative charge of the clay mineral, are either specifically adsorbed or located in the diffuse layer. Therefore, the equilibria at the basal sites are, for example:

$$S + Na^+ = SNa^+: \qquad K_1 \qquad \text{A-23}$$

$$S + Cl^- = SCl^-: \qquad K_2 \qquad \text{A-24}$$

where S is the surface site. The sites available for specific adsorption are assumed to be associated with the charges due to isomorphic substitution:

$$[S] = \sigma_o/F \qquad \text{A-25}$$

where σ_o is the isomorphic-substitution charge density, F is the Faraday constant, and [ ] indicate concentration. Writing the potential at the inner Helmholtz plane as Ψ_β, the mass-action equations become:

$$[SNa^+] = K_1[S][Na^+] \exp(-e\Psi_\beta/kT) \qquad \text{A-26}$$

$$[SCl^-] = K_2[S][Cl^-] \exp(e\Psi_\beta/kT) \qquad \text{A-27}$$

where $K_1$and K_2 are stability constants; e is the protonic charge, and kT is the thermal energy. The Boltzmann-distribution factors describe the effect of the electric potential on the equilibria. The

magnitude of the charge density in the inner Helmholtz plane, σ_β, is a function of the concentration of the different interface species:

$$\sigma_\beta = F \{[SNa^+] - [SCl^-]\} \qquad \text{A-28}$$

The charge located in the diffuse double layer is similarly a function of the species concentration. The determination of all parameters follows the TLM approach. Further, the bulk solution will satisfy the electroneutrality equation:

$$[Na^+] - [Cl^-] + [H^+] - [OH^-] = 0 \qquad \text{A-29}$$

Operationally a value of 0.2 F/m^2 for C_2 and the measured zeta potential for Ψ_d are used. The edge site-adsorption model adopts the TLM as described in section A.2.3.

A.5 References

Adamson, A.W. 1990. *Physical Chemistry of Surfaces.* 5th ed. New York, NY: John Wiley & Sons, Inc.

Allard, B., G.W. Beall, and T. Krajewski. 1980. "The Sorption of Actinides in Igneous Rocks," *Nuclear Technology.* Vol. 49, no. 3, 474-480.

Babcock, K.L. 1963. "Theory of the Chemical Properties of Soil Colloidal Systems at Equilibrium," *Hilgardia.* Vol. 34, 417-418.

Bailey, S.W. 1980. "Summary of Recommendations of AIPEA Nomenclature Committee on Clay Minerals," *American Mineralogist.* Vol. 65, no. 1-2, 1-7.

Davis, J.A., and J.O. Leckie. 1978. "Surface Ionization and Complexation at the Oxide/Water Interface. 2. Surface Properties of Amorphous Iron Oxyhydroxide and Adsorption of Metal Ions," *Journal of Colloid and Interface Science.* Vol. 6, no. 1, 90-107.

Davis, J.A., R.O. James, and J.O. Leckie. 1978. "Surface Ionization and Complexation at the Oxide/Water Interface. 1. Computation of Electrical Double Layer Properties in Simple Electrolytes," *Journal of Colloid and Interface Science.* Vol. 63, no. 3, 480-499.

Dzombak, D.A., and F.M.M. Morel. 1986. "Sorption of Cadmium on Hydrous Ferric Oxide at High Sorbate/Sorbent Ratios: Equilibrium, Kinetics, and Modeling," *Journal of Colloid and Interface Science.* Vol. 112, no. 2, 588-598.

Gast, R.G., and W.D. Klobe. 1971. "Sodium-Lithium Exchange Equilibria on Vermiculite at 25°C and 50°C," *Clays and Clay Mineralogy.* Vol. 19, no. 5, 311-319.

Hayes, K.F., A.L. Roe, G.E. Brown, Jr., K.O. Hodgson, J.O. Leckie, and G.A. Parks. 1987. "In Situ X-Ray Absorption Study of Surface Complexes at Oxide/Water Interfaces: Selenium Oxyanions on α-FeOOH," *Science.* Vol. 238, no. 4828, 783-786.

Healy, T.W., D.E. Yates, L.R. White, and D. Chan. 1977. "Nernstian and Non-Nernstian Potential Differences at Aqueous Interfaces," *Journal of Electroanalytical Chemistry and Interfacial Electrochemistry.* Vol. 80, no. 1, 57-66.

Hohl, H., and W. Stumm. 1976. "Interaction of Pb2+ with Hydrous γ-Al2O3," *Journal of Colloid and Interface Science.* Vol. 55, no. 2, 281-288.

Huang, C.P. 1981. "The Surface Acidity of Hydrous Solids," *Adsorption of Inorganics at Solid-Liquid Interfaces.* Eds. M.A. Anderson and A.J. Rubin. Ann Arbor, MI: Ann Arbor Sci. Pub., Inc. 183-217.

James, R.O., and G.A. Parks. 1982. "Characterization of Aqueous Colloids by Their Electrical Double-Layer and Intrinsic Surface Chemical Properties," *Surface and Colloid Science.* Ed. E. Matijevic. Vol. 12, 119-216.

Jardine, P.M., and D.L. Sparks. 1984. "Potassium-Calcium Exchange in a Multireactive Soil System. II. Thermodynamics," *Soil Science Society of America Journal.* Vol. 48, no. 1, 45-50.

Kleijn, W.B. 1981. "The Physical Chemistry of Clays and Oxides." Ph.D. Dissertation. Riverside, CA: University of California, Riverside.

Levine, S. 1971. "Adsorption Isotherms in the Electrical Double Layer and the Discreteness-of-Charge Effect," *Journal of Colloid and Interface Science.* Vol. 37, no. 3, 619-634.

Lippmann, F. 1954. "Uber Einen Keuperton Von Zaisers Weiher Bei Maulbronn," *Heidelberger Beitrage zur Mineralogie und Petrographie.* Bd. 4, H. 1-2, 130-134.

Singh, V., and G. Uehara. 1986. "Electrochemistry of the Double-Layer: Principles and Applications to Soils," *Soil Physical Chemistry.* Ed. D.L. Sparks. Boca Raton, FL: CRC Press, Inc. 1-38.

Sparks, D. L. 1986. *Soil Physical Chemistry.* Boca Raton, FL: CRC Press, Inc.

Sposito, G. 1984. *The Surface Chemistry of Soils.* New York, NY: Oxford University Press.

Westall, J., and H. Hohl. 1980. "A Comparison of Electrostatic Models for the Oxide/Solution Interface," *Advances in Colloid and Interface Science.* Vol. 12, no. 4, 265-294.

Yates, D.E., S. Levine, and T.W. Healy. 1974. "Site-Binding Model of the Electrical Double-Layer at the Oxide/Water Interface," *Journal of the Chemical Society. Faraday Transactions.* Vol. 70, no. 10, 1807-1818.

APPENDIX B:
MINERALOGICAL STUDIES OF REFERENCE CORRENSITE FROM THE WIPP

APPENDIX B:
MINERALOGICAL STUDIES OF REFERENCE CORRENSITE FROM THE WIPP

Detailed mineralogical studies of the matrix and fracture-fill materials of a large number of samples from the Culebra Dolomite and from clay-rich layers within the Tamarisk Member and the unnamed lower member of the Rustler Formation have been carried out by Sewards et al. (1992). Because only small amounts of clay can be sampled from the Culebra fracture coatings, initial technique and model development for the sorption studies were carried out with a reference corrensite (CorWIPP) from a black shale layer in the upper Tamarisk (Sample ID: AIS-15). The samples were obtained in the Air Intake Shaft from a layer directly underneath the Culebra Dolomite and are described in Sewards et al. (1992). Additional characterization of the reference corrensite CorWIPP by analytical electron microscopy and cation exchange has been described by Krumhansl et al. (1990). These studies are summarized below and provide the basis for comparison of the properties of the corrensite in the Culebra to those of the CorWIPP reference corrensite.

B.1 Methods

B.1.1. X-ray Diffraction

Samples were analyzed with a Scintag PAD-V x-ray diffractometer using CuK_{α} radiation. Whole rock samples were analyzed to determine the major mineral components. Samples containing sulfates and carbonates were treated with disodium-ethylenediamine tetraacetic acid (EDTA) to remove these salts. The <2 micron fraction was separated by centrifugation and oriented clay aggregates were prepared by the filter transfer method. Oriented mounts were either glycolated or heated to 250°, 500°, or 650°C and analyzed from 2 to 30° 2-theta. Clay minerals were identified by standard techniques (Brindley and Brown, 1980). Quantitative analysis of individual clay minerals was performed using the method of Reynolds (1985). Additional details of the x-ray analysis and data reduction techniques are found in Sewards et al. (1992).

B.1.2 Bulk Chemistry and Microchemistry

Oxide analyses of the <2 micrometer fraction were made by atomic absorption spectroscopy. Chemical composition of individual clay crystallites was obtained by energy dispersive spectroscopy (EDS) on transmission electron microscopes. Transmission electron micrograph and high resolution transmission electron microscopy (TEM) images of individual clay particles from the CorWIPP are described by Krumhansl et al. (1990) and Sewards et al. (1992), respectively. Details of sample preparation, electron microscopy, and elemental microanalysis can be found in these papers.

B.1.3 Cation Exchange Capacity

Cation exchange capacity (CEC) was measured by two methods. Sewards et al. (1992) used the sodium acetate method wherein the samples were saturated with Na-acetate, washed in ethyl alcohol, and resaturated with ammonium acetate. The CEC is calculated from the Na concentration of the supernatant. Krumhansl et al. (1990) used a Mg-Ca exchange method. The sample was washed free of soluble salts, repeatedly washed with 0.5 N $CaCl_2$ to saturate exchange sites with Ca^{2+}, and then washed repeatedly with 0.5 N $MgCl_2$ to remove the Ca^{2+}. The CEC was calculated from the concentration of Ca^{2+} in the supernatant.

B.2 Results

B.2.1 Compositions of Corrensite from CorWIPP and other Samples

Chemical compositions of the CorWIPP samples and several other clay separates are listed in Table B-1. Using x-ray diffraction (XRD), Sewards et al. (1992) determined that the CorWIPP sample contained 94% corrensite. Structural formulae calculated from clay separates using XRD and atomic absorption data are shown in Table B-2. The formulae for CorWIPP (AIS-15) are compared to those from corrensite from a claystone sample from the Tamarisk (R35) and from a clay-rich dolomite from the Culebra (CS-7).

B.2.2 Morphology and Composition of Clay Crystallites

Krumhansl et al. (1990) observed a mixture of morphologic and compositional groups in clay fractions from CorWIPP with analytical transmission electron microscopy. Irregular platelets, up to several microns in diameter with low Fe contents (3.1 and 4.4 wt%) and average Fe/K wt% ratios of 0.67, were tentatively identified as illite. Platelets with similar size range, but with higher Fe contents (20-28.4 wt%) and average Fe/K ratio of 5.9, were tentatively identified as chlorite. A fine-grained crystalline material with no discernible morphology at a resolution of 30 nm was tentatively identified as corrensite. The composition of this material is listed in Table B-1.

Table B-1. Chemical Analyses of CorWIPP and Other Clay Samples Containing Corrensite

Sample	SiO_2	Al_2O_3	TiO_2	FeO	MgO	CaO	Na_2O	K_2O	Total	%Cr[1]	M[2]
CorWIPP (AIS-15)	43.05	13.08	0.41	3.24	26.35	0.20	0.44	1.57	88.31	94	A
CorWIPP (Clay P)[3]	42.9	13.4	0.0	2.7	39.0	1.2	0.0	0.9	100.1	–	T
CS-7	36.10	12.00	–	3.10	26.00	0.10	0.18	1.78	79.17	36	A
AIS-17	45.97	10.35	–	3.64	29.22	0.09	0.04	0.79	90.09	75	A
R-35	32.50	17.00	0.15	15.0	11.80	0.09	0.45	0.72	77.71	61	M

[1]Percent corrensite in sample as determined by XRD.

[2]M: analytical methods: A = bulk composition by atomic absorption (Sewards et al., 1992); T = analytical TEM with energy dispersive analysis; M = electron microscope (Sewards et al., 1992); average of 15 analyses.

[3]Data from Krumhnansl et al., 1990; average composition from analytical TEM.

Table B-2. Structural Formulae* for Corrensites and Reference Clays**

Sample (ref)	Tetrahedral sites		Octahedral sites			Interlayer sites		
	Si	Al	Mg	Fe	Al	Ca	Na	K
AIS–15 (1)	14.09	1.91	12.86	0.89	3.13	0.07	0.22	0.66
AIS–15 (2)	13.87	2.13	14.57	0.44	2.37	0.27	0.00	0.21
CS–7 (1)	13.26	2.74	14.24	0.92	2.46	0.04	0.10	0.83
R–35 (1)	12.89	3.11	6.98	4.97	4.83	0.04	0.27	0.36
AIS–17 (3)	14.67	1.33	13.01	1.09	2.93	0.00	0.04	0.15

* Structural formulae corresponding to reference unit cell composition:
$[int.]_{0.4}\,[oct.]_{18}\,[tet.]_{16}\,O_{40}(OH)_{20}$

** References:

(1) Sewards et al. (1992): formula calculated from bulk chemical analyses of clay separates. R-35 (Well W-19) is from a claystone sample from the Tamarisk Member; CS-7 (Well W-28) is a clay-rich dolomite from the Culebra Dolomite; AIS-15 is the CorWIPP reference obtained from the black shale layer of the unnamed member directly underlying the Culebra in the Air Intake Shaft.

(2) Krumhansl et al. (1990): formula calculated from analytical electron microscopy (AEM/EDS) analyses of crystalline fines component of their Clay P sample from the CorWIPP reference. Sample was washed with 0.5 N $CaCl_2$ solution prior to analyses to saturate all exchangeable sites with Ca^{2+}.

(3) Sewards et al. (1992): calculated from EDS analyses obtained during TEM study of clay particles from the red shale layer of the unnamed member that directly underlies the black shale (CorWIPP) horizon described above.

High resolution TEM images of corrensite intercalated with tetradecyl ammonium chloride were obtained on CorWIPP and other samples by Sewards et al. (1992). A striking feature of corrensite morphology is its strong resemblance to dioctahedral smectite (montmorillonite) morphology. Regular alternation of 1.4 and 1.8 nm layers was observed, corresponding to the chlorite and saponite layers, respectively. EDS spectra of the crystallites show the presence of Mg, Al, Si, and Fe. The amount of Fe is variable; there appear to be two distinct families of composition, one with high Fe and one with low Fe content.

Table B.2 contains an average structural formula that was calculated from data for six crystallites from the CorWIPP sample obtained on the TEM by EDS analysis (Krumhansl et al., 1990). In addition, Table B.2 contains an average structural formula that was calculated from TEM analyses of crystallites of corrensite from a red shale layer (AIS-17) in the unnamed member (Sewards et al., 1992). This unit underlies the black shale from which the CorWIPP sample was taken. Samples R-35 and CS-7 are clay-rich samples from the Tamarisk and Culebra members, respectively.

B.2.3 Cation Exchange Capacity

A CEC of 85 meq/100g for the CorWIPP reference was determined using the sodium acetate exchange method (Sewards et al., 1992). A relationship between the corrensite content and CEC was observed for a suite of seven clay mineral separates, including the CorWIPP and six samples from the Culebra. This is to be expected because the CEC of corrensite, which contains expandable layers, is much higher than the other component clay minerals (illite, serpentine, or chlorite).

Krumhansl et al. (1990) also observed a relationship between CEC and the proportion of corrensite in a suite of samples taken from the Salado and Rustler formations. They measured a CEC of 31 meq/100g for CorWIPP using the Mg-Ca exchange method. For comparison, they calculated an exchange capacity of their idealized corrensite formula in Table B.2 to be 43 meq/100g.

It is not known why the work of Sewards et al. (1992) and Krumhansl et al. (1990) yielded such different estimates of the CEC of the CorWIPP sample. Two possible reasons are that Na-containing evaporite salts or excess disodium EDTA was present in the samples analyzed by Sewards using the Na-acetate exchange method and that Mg-Ca exchange was not carried to

completion by Krumhansl et al. The former would lead to an apparently high CEC, whereas the latter would result in a low CEC.

B.3 Summary

Only small amounts of clay can be sampled from the Culebra fracture coatings and matrix; therefore, initial technique and model development for the uranyl sorption studies were carried out with a reference corrensite (CorWIPP) from a black shale layer in the upper Tamarisk. The samples were obtained in the Air Intake Shaft from a layer directly underneath the Culebra Dolomite. Characteristics of the reference corrensite CorWIPP as determined by XRD, atomic absorption, analytical electron microscopy, and cation exchange studies are similar to those of the corrensite in the Culebra Dolomite.

B.4 References

Brindley, G.W., and G. Brown, eds. 1980. *Crystal Structures of Clay Minerals and Their X-Ray Identification.* London: Mineralogical Society.

Krumhansl, J.L., K.M. Kimball, and C.L. Stein. 1990. *A Review of WIPP Repository Clays and Their Relationship to Clays of Adjacent Strata.* SAND90-0549. Albuquerque, NM: Sandia National Laboratories.

Reynolds, R.C., Jr. 1985. "Principles and Techniques of Quantitative Analysis of Clay Minerals by X-Ray Powder Diffraction," *Quantitative Mineral Analysis of Clays.* Eds. D.R. Pevear and F.A. Mumpton. CMS Workshop Lectures Vol. 1. Evergreen, CO: The Clay Minerals Society. 4-36.

Sewards, T., A. Brearley, R. Glenn, I.D.R. MacKinnon, and M.D. Siegel. 1992. *Nature and Genesis of Clay Minerals of the Rustler Formation in the Vicinity of the Waste Isolation Pilot Plant Southeastern New Mexico.* SAND90-2569. Albuquerque, NM: Sandia National Laboratories.

APPENDIX C:
ADSORPTION OF URANYL ONTO VARIOUS CONTAINER MATERIALS

APPENDIX C:
ADSORPTION OF URANYL ONTO VARIOUS CONTAINER MATERIALS

Tables C-1 through C-5 contain a summary of the results of attempts to determine the extent to which various container surfaces sorb trace amounts of U(VI). Depending on the container and pH, sorption ranged from nil to 100%. Since fractional U(VI) adsorption increases with pH, the most critical test of container sorption is at neutral to high pH.

Table C-1. Container Adsorption: 40 mL Capacity Glass and Polypropylene Centrifuge Tubes

Experimental Conditions: $U(VI)_T = 4.2 \times 10^{-7}$ M
$I = 0.1$ M $NaClO_4$
$V_T = 10$ mL
25°C

Sample #	pH_f	Data *	Conc. ($\times 10^{-7}$ M)	% Loss
Glass				
1	4.6	37	3.86	8
2	3.9	31	3.28	22
3	3.3	28	2.94	30
4	6.3	19	2.02	52
5	7.7	26	2.73	35
6	8.5	16	1.68	60
7	9.6	25	2.65	37
Polypropylene				
1	4.6	36	3.78	10
2	3.9	40	4.2	0
3	3.3	41	4.2	0
4	6.3	27	2.86	32
5	7.7	29	3.07	27
6	8.5	34	3.57	15
7	9.6	33	3.49	17

*Standard reading for 4.2×10^{-7} M is 40 ± 1.

Table C-2. Comparison of Sorption onto Various Container Surfaces with $U(VI)_T = 4.2 \times 10^{-7}$ M

Experimental Conditions: $U(VI)_T = 4.2 \times 10^{-7}$ M
$I = 0.1$ M $NaClO_4$
$V_T = 10$ mL
25°C

Sample #	pH_f	Data *	% Loss
Polypropylene			
1	3.3	50	0
2	5.5	41	17.4
3	7.0	22	55.4
4	9.9	50	0
Polycarbonate			
1	3.3	52	0
2	5.5	50	0
3	7.0	47	7
4	9.3	48	4.4
Low density polyethylene			
1	3.3	55	0
2	5.5	46	8.4
3	7.0	50	1
4	10.0	55	0
High density polyethylene			
1	3.3	56	0
2	7.0	44	12
Teflon			
1	6.9	49	3

*Standard reading is 50 ± 3.

Note: All experiments were carried out at lower head space by introducing 100 mL solution to 125 mL capacity containers.

Table C-3. Comparison of Sorption onto Various Container Surfaces with U(VI) = 4.2×10^{-6} M

Experimental Conditions: U(VI) = 4.2×10^{-6} M
I = 0.1 M $NaClO_4$
25°C

Sample #	pH_f	Data *	% Loss
Polypropylene			
1	3.8	>50	0
2	4.9	>50	0
3	7.4	48	18
4	8.5	47	19
Polycarbonate			
1	3.8	>50	0
2	4.6	>50	0
3	6.3	>50	0
4	7.1	>50	0
Low density polyethylene			
1	3.8	>50	0
2	4.8	>50	0
3	6.6	>50	0
4	8.2	>50	0
High density polyethylene			
1	7.3	>50	0
2	8.1	>50	0
Teflon			
1	7.3	>50	0

*Standard reading is 50 ± 3.

Note: Higher surface loading was tested. All containers except for polypropylene showed good results.

Table C-4. Comparison of Selected Container Materials

Experimental Conditions: $U(VI) = 10^{-6}$ M
$I = 0.1$ M $NaClO_4$
$V_T = 35$ mL
25°C
25°C

Sample #	pH_f	Data	% Loss
Polycarbonate			
1	3.8	>54	0
2	4.4		
3	4.6	>54	0
4	5.0	>52	3.7
5	5.9	>54	0
6	6.2	>54	0
7	6.4	>54	0
8	7.1	50	7.4
9	7.3	>54	0
10	9.3	53	1.9
		(standard reading 54)	
Low density polythylene			
1	3.8	>50	0
2	4.4	47	6
3	4.6	48	4
4	5.0	>50	0
5	5.9	48	4
6	6.2	>50	0
7	6.4	>50	0
8	7.1	>50	0
9	7.3	48	4
10	8.3	49	2
		(standard reading 50)	
Polyallomer			
1	3.8	>56	0
2	4.4	>56	0
3	4.6	>56	0
4	5.1	51	9
5	6.1	44	21.4
6	6.6	56	0
7	7.2	>56	0
8	7.7	>56	0
9	9.2	56	0
		(standard reading 56)	

Note: According to above data, polycarbonate and low density polyethylene containers are the most suitable. We chose to use polycarbonate because polyethylene centrifuge tubes do not come with screw caps.

Table C-5. Confirmation of Selecting Sorption-free Container

Experimental Conditions: $U(VI) = 10^{-6}$ M
$I = 0.01$ M $NaClO_4$
S = 0.1 g/L CorWa
25°C

Sample #	pH_f	Data	% Loss
35 mL polycarbonate			
1	4.1	47	15
2	4.5	43	23
3	5.1	32	42
4	5.6	24	57
5	6.3	23	59
6	6.7	40	28
7	7.3	34	39
8	8.2	49	12
9	9.5	49	12
10	10.6	>55	0

Note: The fact that loss of U(VI) in the presence of CorWa in 50 mL test tube is equivalent to or less than that in 100 mL bottles confirms that polycarbonate containers are free from container wall adsorption.

APPENDIX D: URANYL ANALYSIS

APPENDIX D: URANYL ANALYSIS

D.1 Method Description

The stable oxidation state of uranium is U(VI) in oxygenated waters and its predominant form is the uranyl ion (UO_2^{2+}). Several techniques have been developed for the determination of U(VI) in water including spectrophotometry (Florence and Farrer, 1963), neutron activation (Holzbecher and Ryan, 1980), gas chromatography (Sieck et al., 1971), and pulse polarography (Milner et al., 1961). These techniques are not sufficiently sensitive for the direct determination of U(VI) below 10^{-8} M.

Analysis by Differential Pulse Cathodic Stripping Voltammetry (DPCSV) is most frequently used for the determination of trace metal ions. This method allows direct analysis of very dilute solution (down to 10nM-0.1nM). The DPCSV method is essentially a 2-stage process: deposition of U(VI) from solution onto a hanging mercury drop electrode (HMDE) and cathodic stripping of deposited species by increasing the potential at a constant rate. Most experimental steps used here were the same as the method described by Van den Berg and Nimmo (1987).

A PAR 174A Polarograph with a PAR 303A Static Mercury Drop Electrode, Omnigraphic 2000 X-Y Recorder (Houston Instrument), and a PAR 315 Electronic Magnetic Stirrer were used for analysis. Potentials are given with respect to an Ag/AgCl, saturated KCl, reference electrode. The working uranyl solution was prepared by diluting a commercially standardized 1000 ppm stock uranyl nitrate solution (Anderson Laboratories; available through VWR Scientific). An aqueous stock solution of 0.1 M oxine in 0.25 M HCl was prepared by dissolving the weighed amount of chemical (Matheson Coleman & Bell) with distilled deionized water and acid in a volumetric flask and diluting. An aqueous pH buffer stock solution was prepared by dissolving the weighed amount needed to make 1M PIPES [piperazine-N, -N'-bis (2-ethanesulfonic acid), bisodium salt, Aldrich Chemical Comp.] and by adding drops of 1 M HCl until a pH of 7 was reached. (Care should be taken not to exceed the mark of the flask in dissolving solid PIPES.) The pH was measured by the Orion Microprocessor Ionalyzer/901 calibrated at pH 7 and 10. 0.1 M ethylenediaminetetraacetic acid (EDTA) stock solution was prepared from its sodium form (Aldrich Chemical Comp.).

A 10-mL sample aliquot was pipetted into the voltammetric cell, and 0.1 mL of PIPES buffer (final concentration, 0.01 M) and 0.02 mL of 0.01 M oxine solution (final concentration,

2 x 10^{-5} M) were added. 0.01 mL of 0.1 M EDTA was added to avoid interference of other metals such as lead and cadmium. The presence of oxygen in the sample solution caused significant interference with the polarographic determination. Purging was accomplished by sending oxygen-free nitrogen gas (ultra pure 99.999% obtained from Liquid Carbonic Inc.) through a dip tube. Four-minute purging was sufficient to remove the dissolved oxygen.

After deaeration of the solution, the potentiostat and the stirrer were switched to -0.3 V and slow mode, respectively, and a new mercury drop was extruded, which signified the beginning of the adsorption period. Various adsorption potentials were tested. This electrodeposition step was carried out by adsorbing the U(VI)-oxine complex onto the surface of the mercury electrode. Stirring stopped after a preselected time (depending on the U(VI) concentration). The solution was allowed to become quiescent for 10 seconds. The concentration of metal in the amalgam became more uniform during the quiescent period. This step was followed by a linear potential sweep stripping step. The Cathodic Stripping Voltammetry (CSV) scan was started. During this step, the sorbed electroactive U(VI) was reduced to U(V) with the transfer of one electron from the Hg electrode to the sorbed U(VI)-oxine when the applied sorption potential was made increasingly more negative by application of a linear ramp potential-time function.

A typical peak-shaped current-voltage curve was obtained; the peak-height or area was a measure of the solution concentration of the sorbed electroactive species. The measurement was repeated after a standard addition of uranium to the sample. For samples ranging from 1 to 100 nM, high sensitivity was observed with one-minute stirring. The peak current-uranium concentration response was linear down to 1 nM. The analytical conditions are shown in Table 2.1. Most correlation coefficients of standard calibrations for experiments were greater than 0.97. The precision for each sample was typically < 10% at U(VI) concentrations of 10^{-6} M. However, the error range may increase when U(VI) concentrations < 10^{-7} M are analyzed.

APPENDIX E:
EXPERIMENTAL DATA FROM EQUILIBRIUM ADSORPTION STUDIES

APPENDIX E:
EXPERIMENTAL DATA FROM EQUILIBRIUM ADSORPTION STUDIES

Experimental Conditions: Corrensite: 0.1 g/L, I: 0.01 M $NaClO_4$, U(VI): 10^{-6} M

pH	U(VI) remaining in solution (x 10^{-7} M)	% U(VI) adsorbed
4.50	2.95	70.5
5.00	1.26	87.4
5.60	0	100.0
5.70	0	100.0
6.00	0	100.0
6.10	0	100.0
6.20	0	100.0
6.40	0	100.0
6.60	0	100.0
6.70	0	100.0
6.80	0	100.0
7.20	0.84	91.6
7.30	1.26	87.4
7.80	2.11	78.9
8.20	2.95	70.5
8.70	2.74	72.6

Experimental Conditions: Corrensite: 0.1 g/L, I: 0.01 M $NaClO_4$, U(VI): 10^{-6} M

pH	U(VI) remaining in solution (x 10^{-7} M)	% U(VI) adsorbed
4.10	7.42	25.8
4.20	8.58	14.2
4.50	5.76	42.4
4.60	6.66	33.4
4.70	6.07	39.3
4.90	3.85	61.5
5.00	4.7	53.0
5.10	4.29	57.1
5.30	3.99	60.1
5.30	2.07	79.3
5.40	4.39	56.1
5.60	1.92	80.8
6.20	1.52	84.8
6.40	2.42	75.8
6.40	2.58	74.2
6.80	2.27	77.3
7.00	3.18	68.2
7.30	3.64	63.6
8.20	4.55	54.5
8.00	5.15	48.5
8.60	6.67	33.3
8.80	6.21	37.9

Experimental Conditions: Corrensite: 0.1 g/L, I: 0.01 M $NaClO_4$, U(VI): 10^{-6} M

pH	U(VI) remaining in solution (x 10^{-7} M)	% U(VI) adsorbed
4.15	6.77	32.3
4.55	6.05	39.5
5.15	4.29	57.1
6.05	2.72	72.8
6.35	3.6	64.0
6.60	4.29	57.1
7.70	7.44	25.6

Experimental Conditions: Corrensite: 0.1 g/L, I: 0.01 M $NaClO_4$, U(VI): 10^{-6} M

pH	U(VI) remaining in solution (x 10^{-7} M)	% U(VI) adsorbed
6.70	6.74	32.6
7.50	8.42	15.8
7.70	8.84	11.6
8.10	8.0	20.0
8.30	10.0	0
8.90	10.0	0

Experimental Conditions: Corrensite: 0.1 g/L, I: 0.01 M $NaClO_4$, U(VI): 10^{-6} M

pH	U(VI) remaining in solution (x 10^{-7} M)	% U(VI) adsorbed
4.10	7.16	28.4
4.20	5.68	43.2
4.20	6.11	38.9
4.40	6.11	38.9
4.90	4.42	55.8
5.70	4.63	53.7
6.10	4.0	60.0
6.20	3.58	64.2
6.50	4.42	55.8
6.70	3.79	62.1
6.70	5.05	49.5
6.90	5.47	45.3
6.90	5.89	41.1
7.20	5.89	41.1
7.50	8.21	17.9
8.50	9.26	7.4
9.50	10.0	0

Experimental Conditions: Corrensite: 0.1 g/L, I: 0.01 M $NaClO_4$, U(VI): 10^{-6} M

pH	U(VI) remaining in solution (x 10^{-7} M)	% U(VI) adsorbed
4.20	8.58	14.2
4.60	6.66	33.4
4.70	6.07	39.3
4.90	3.85	61.5
5.10	4.29	57.1
5.30	3.99	60.1
5.30	2.07	79.3
5.60	1.92	80.8
7.00	2.07	79.3
5.90	1.18	88.2
6.00	1.78	82.2
6.10	1.18	88.2
6.20	1.18	88.2
6.20	1.18	88.2
6.60	1.63	83.7
8.20	6.05	39.5

Experimental Conditions: Corrensite: 0.1 g/L, I: 0.01 M $NaClO_4$, U(VI): 10^{-6} M

pH	U(VI) remaining in solution (x 10^{-7} M)	% U(VI) adsorbed
4.18	8.06	19.4
4.20	6.53	34.7
4.50	5.14	48.6
4.80	2.08	79.2
5.30	2.22	77.8
5.60	1.11	88.9
6.00	1.94	80.6
6.10	1.11	88.9
6.40	1.11	88.9
7.10	4.44	55.6
8.10	3.89	61.1
8.30	6.11	38.9
8.70	8.19	18.1
8.80	7.36	26.4

Experimental Conditions: Corrensite: 0.1 g/L, I: 0.01 M $NaClO_4$, U(VI): 10^{-6} M

pH	U(VI) remaining in solution (x 10^{-7} M)	% U(VI) adsorbed
4.30	5.33	46.7
4.50	3.85	61.5
4.60	2.66	73.4
5.10	2.66	73.4
5.20	2.07	79.3
5.40	2.51	74.9
5.70	1.92	80.8
5.80	1.78	82.2
5.90	1.78	82.2
6.00	1.48	85.2
6.10	1.63	83.7
6.30	1.48	85.2
6.40	2.22	77.8
6.50	2.66	73.4
6.60	2.22	77.8
6.70	2.81	71.9
6.90	2.81	71.9
7.10	3.7	63.0
9.00	6.95	30.5

Experimental Conditions: Corrensite: 0.1 g/L, I: 0.01 M $NaClO_4$, U(VI): 10^{-6} M

pH	U(VI) remaining in solution (x 10^{-7} M)	% U(VI) adsorbed
4.20	5.29	47.1
4.60	6.08	39.2
4.80	5.16	48.4
5.00	2.51	74.9
5.40	2.25	77.5
6.00	2.38	76.2
7.30	3.44	65.6
8.30	3.57	64.3
9.00	3.44	65.6

Experimental Conditions: Corrensite: 0.1 g/L, I: 0.01 M $NaClO_4$, U(VI): 10^{-6} M

pH	U(VI) remaining in solution (x 10^{-7} M)	% U(VI) adsorbed
4.10	8.54	14.6
4.30	5.49	45.1
4.50	4.27	57.3
5.40	1.34	86.6
6.40	1.71	82.9
6.50	1.95	80.5
6.60	2.2	78.0
6.80	2.44	75.6
6.80	2.68	73.2
7.10	2.78	72.2
7.20	2.59	74.1
7.20	2.96	70.4
7.50	3.52	64.8
7.70	3.15	68.5
8.00	3.52	64.8
8.20	4.81	51.9
8.40	4.07	59.3

Experimental Conditions: Corrensite: 0.1 g/L, I: 0.01 M $NaClO_4$, U(VI): 10^{-6} M

pH	U(VI) remaining in solution (x 10^{-7} M)	% U(VI) adsorbed
4.30	8.18	18.2
4.40	7.09	29.1
4.50	6.91	30.9
4.60	6.18	38.2
4.80	4.0	60.0
4.80	5.09	49.1
5.00	3.27	67.3
5.30	2.55	74.5
5.90	2.91	70.9
6.20	3.64	63.6
6.50	2.73	72.7
6.80	4.55	54.5
7.80	6.18	38.2
8.40	5.27	47.3
9.00	10.0	0

Experimental Conditions: Corrensite: 0.1 g/L, I: 0.01 M $NaClO_4$, U(VI): 10^{-6} M

pH	U(VI) remaining in solution (x 10^{-7} M)	% U(VI) adsorbed
4.30	5.5	45.0
4.80	2.15	78.5
5.10	1.74	82.6
5.60	1.74	82.6
5.90	1.61	83.9
6.30	1.61	83.9
6.50	1.88	81.2
6.60	1.88	81.2
6.70	2.55	74.5
6.90	3.22	67.8
6.80	2.15	78.5
7.00	2.15	78.5
7.50	3.09	69.1
8.00	4.97	50.3
7.50	4.83	51.7
7.60	4.83	51.7
8.10	6.44	35.6
8.90	5.91	40.9
8.90	6.98	30.2
9.00	5.77	42.3

Experimental Conditions: Corrensite: 0.1 g/L, I: 0.01 M $NaClO_4$, U(VI): 10^{-6} M

pH	U(VI) remaining in solution (x 10^{-7} M)	% U(VI) adsorbed
4.30	8.36	16.4
4.50	8.91	10.9
4.60	7.82	21.8
4.80	5.45	45.5
5.00	5.45	45.5
5.20	5.09	49.1
5.20	5.64	43.6
5.40	6.0	40.0
5.60	5.09	49.1
5.90	3.64	63.6
6.30	2.91	70.9
6.50	4.18	58.2
7.00	5.82	41.8
7.50	6.0	40.0
8.70	7.27	27.3
9.10	9.64	3.6

Experimental Conditions: Corrensite: 0.1 g/L, I: 0.01 M $NaClO_4$, U(VI): 10^{-6} M

pH	U(VI) remaining in solution (x 10^{-7} M)	% U(VI) adsorbed
4.30	4.21	57.9
4.50	3.68	63.2
4.60	3.68	63.2
4.60	2.89	71.1
4.80	2.37	76.3
5.00	1.97	80.3
5.30	2.11	78.9
5.00	1.45	85.5
5.40	1.97	80.3
5.60	1.32	86.8
6.30	2.63	73.7
6.10	1.18	88.2
6.20	1.18	88.2
6.50	1.58	84.2
7.40	4.71	52.9
8.60	6.96	30.4
8.60	7.39	26.1
9.00	8.12	18.8

WIPP
UC721 - DISTRIBUTION LIST

Federal Agencies

US Department of Energy (6)
Office of Civilian Radioactive Waste Mgmt.
Attn: Deputy Director, RW-2
Associate Director, RW-10/50
Office of Prog. & Resources Mgmt.
Office of Contract Business Mgmt.
Director, RW-22
Analysis & Verification Division
Associate Director, RW-30
Office of Systems & Compliance
Associate Director, RW-40
Office of Storage & Transportation
Director, RW-4/5
Office of Strategic Planning and International Programs
Office of External Relations
Forrestal Building
Washington, DC 20585

US Department of Energy
Albuquerque Operations Office
Attn: National Atomic Museum Library
P.O. Box 5400
Albuquerque, NM 87185-5400

US Department of Energy
Research & Waste Management Division
Attn: Director
P.O. Box E
Oak Ridge, TN 37831

US Department of Energy (6)
Carlsbad Area Office
Attn: V. Daub
G. Dials
M. McFadden
R. Lark
R. Bills
J. A. Mewhinney
P.O. Box 3090
Carlsbad, NM 88221-3090

US Department of Energy
Attn: E. Young
Room E-178
GAO/RCED/GTN
Washington, DC 20545

US Department of Energy (3)
YMPO
Attn: Dr. Ardyth Simmons
101 Convention Center Drive
Las Vegas, NV 89109

US Department of Energy
Office of Environmental Restoration and Waste Management
Attn: J. Lytle, EM-30
Forrestal Building
Washington, DC 20585-0002

US Department of Energy (3)
Office of Environmental Restoration and Waste Management
Attn: M. Frei, EM-34, Trevion II
Washington, DC 20585-0002

US Department of Energy
Office of Environmental Restoration and Waste Management
Attn: S. Schneider, EM-342, Trevion II
Washington, DC 20585-0002

US Department of Energy (2)
Office of Environment, Safety & Health
Attn: C. Borgstrom, EH-25
R. Pelletier, EH-231
Washington, DC 20585

US Department of Energy (2)
Idaho Operations Office
Fuel Processing & Waste Mgmt. Division
785 DOE Place
Idaho Falls, ID 83402

US Environmental Protection Agency (2)
Radiation Protection Programs
Attn: M. Oge
ANR-460
Washington, DC 20460

US Nuclear Regulatory Commission
Division of Waste Management
Attn: H. Marson
Mail Stop 4-H-3
Washington, DC 20555

Office of Nuclear Regulatory Research
Attn: G. F. Birchard
MS NL-005
Washington, DC 20555

Office of Nuclear Regulatory Research
Attn: L. A. Kovach
MS NL-005
Washington, DC 20555

Boards

Defense Nuclear Facilities Safety Board
Attn: D. Winters
625 Indiana Ave. NW, Suite 700
Washington, DC 20004

Nuclear Waste Technical Review Board (2)
Attn: Chairman
S. J. S. Parry
1100 Wilson Blvd., Suite 910
Arlington, VA 22209-2297

Advisory Committee on Nuclear Waste
Nuclear Regulatory Commission
Attn: R. Major
7920 Norfolk Ave.
Bethesda, MD 20814

State Agencies

Attorney General of New Mexico
P.O. Drawer 1508
Santa Fe, NM 87504-1508

Environmental Evaluation Group (3)
Attn: Library
7007 Wyoming NE
Suite F-2
Albuquerque, NM 87109

NM Energy, Minerals, and Natural
Resources Department
Attn: Library
2040 S. Pacheco
Santa Fe, NM 87505

NM Environment Department (3)
Secretary of the Environment
Attn: Mark Weidler
1190 St. Francis Drive
Santa Fe, NM 87503-0968

NM Bureau of Mines & Mineral Resources
Socorro, NM 87801

NM Environment Department
WIPP Project Site
Attn: P. McCasland
P.O. Box 3090
Carlsbad, NM 88221

Laboratories/Corporations

Battelle Pacific Northwest Laboratories
Attn: R. E. Westerman, MSIN P8-44
Battelle Blvd.
Richland, WA 99352

Jan Docka
Roy F. Weston, Inc.
955 L'Enfant Plaza SW
Washington, DC 20024

INTERA, Inc.
Attn: G. A. Freeze
1650 University Blvd. NE, Suite 300
Albuquerque, NM 87102

INTERA, Inc.
Attn: J. F. Pickens
6850 Austin Center Blvd., Suite 300
Austin, TX 78731

INTERA, Inc.
Attn: W. Stensrud
P.O. Box 2123
Carlsbad, NM 88221

Los Alamos National Laboratory
Attn: B. Erdal, INC-12
P.O. Box 1663
Los Alamos, NM 87544

RE/SPEC, Inc
Attn: Angus Robb
4775 Indian School NE, Suite 300
Albuquerque, NM 87110-3927

RE/SPEC, Inc
Attn: J. L. Ratigan
P.O. Box 725
Rapid City, SD 57709

Los Alamos National Laboratory
Attn: Dr. Ines Triay
INC 9 Mail Stop J514
Los Alamos, NM 87545

Oak Ridge National Laboratory
Attn: G. Jacobs
Box 2009
Oak Ridge, TN 37831

Los Alamos National Laboratory
Attn: Dr. Everett Springer
ESS 15 Mail Stop J495
Los Alamos, NM 87545

Center for Nuclear Waste
Regulatory Analyses
Attn: W. Murphy
6220 Culebra Road
Drawer 28510
San Antonio, TX 78284

Center for Nuclear Waste
Regulatory Analyses
Attn: R. Pabalon
6220 Culebra Road
Drawer 28510
San Antonio, TX 78284

Southwest Research Institute (2)
Center for Nuclear Waste Regulatory Analysis
Attn: P. K. Nair
6220 Culebra Road
San Antonio, TX 78228-0510

Tech Reps, Inc. (4)
Attn: J. Chapman (2)
T. Peterson (2)
5000 Marble NE, Suite 222
Albuquerque, NM 87110

Westinghouse Electric Corporation (5)
Attn: Library
C. Cox
L. Fitch
B. A. Howard
R. Kehrman
P.O. Box 2078
Carlsbad, NM 88221

Dr. Stephen Nelson
Woodward Clyde Federal Systems
Yucca Mountain Site Characterization Project
101 Convention Center Drive
Las Vegas, NV 89109

S. Cohen & Associates
Attn: Bill Thurber
1355 Beverly Road
McLean, VA 22101

**National Academy of Sciences,
WIPP Panel**

Howard Adler
Oxyrase, Incorporated
7327 Oak Ridge Highway
Knoxville, TN 37931

Ina Alterman
Board of Radioactive Waste Management
GF456
2101 Constitution Ave.
Washington, DC 20418

Rodney C. Ewing
Department of Geology
University of New Mexico
Albuquerque, NM 87131

Charles Fairhurst
Department of Civil and Mineral Engineering
University of Minnesota
500 Pillsbury Dr. SE
Minneapolis, MN 55455-0220

B. John Garrick
PLG Incorporated
4590 MacArthur Blvd., Suite 400
Newport Beach, CA 92660-2027

Leonard F. Konikow
US Geological Survey
431 National Center
Reston, VA 22092

Carl A. Anderson, Director
Board of Radioactive Waste Management
National Research Council
HA 456
2101 Constitution Ave. NW
Washington, DC 20418

Christopher G. Whipple
ICF Kaiser Engineers
1800 Harrison St., 7th Floor
Oakland, CA 94612-3430

John O. Blomeke
720 Clubhouse Way
Knoxville, TN 37909

Sue B. Clark
University of Georgia
Savannah River Ecology Lab
P.O. Drawer E
Aiken, SC 29802

Konrad B. Krauskopf
Department of Geology
Stanford University
Stanford, CA 94305-2115

Della Roy
Pennsylvania State University
217 Materials Research Lab
Hastings Road
University Park, PA 16802

David A. Waite
CH_2 M Hill
P.O. Box 91500
Bellevue, WA 98009-2050

Thomas A. Zordon
Zordan Associates, Inc.
3807 Edinburg Drive
Murrysville, PA 15668

Universities

University of New Mexico
Geology Department
Attn: Library
141 Northrop Hall
Albuquerque, NM 87131

University of Washington
College of Ocean & Fishery Sciences
Attn: G. R. Heath
583 Henderson Hall, HN-15
Seattle, WA 98195

Penn State University
Attn: Gour-Tsyh Yeh
Professor of Civil Engineering
212 Sacket Bldg.
University Park, PA 16802

Stanford University (10)
Environmental Engineering and Science
Attn: Dr. James O. Leckie
Department of Civil Engineering
Stanford, CA 94305

Libraries

Thomas Brannigan Library
Attn: D. Dresp
106 W. Hadley St.
Las Cruces, NM 88001

Government Publications Department
Zimmerman Library
University of New Mexico
Albuquerque, NM 87131

New Mexico Junior College
Pannell Library
Attn: R. Hill
Lovington Highway
Hobbs, NM 88240

New Mexico State Library
Attn: N. McCallan
Don Gaspar
Santa Fe, NM 87503

New Mexico Tech
Martin Speere Memorial Library
Campus Street
Socorro, NM 87810

WIPP Public Reading Room
Carlsbad Public Library
101 S. Halagueno St.
Carlsbad, NM 88220

Foreign Addresses

Studiecentrum Voor Kernenergie
Centre d'Energie Nucleaire
Attn: A. Bonne
SCK/CEN Boeretang 200
B-2400 Mol, BELGIUM

Dr. Henning von Maravic
Programme Radioactive Waste Mgmt.
Rue de la Loi
Wetstraal 200
8-104 Brussels
BELGIUM

Atomic Energy of Canada, Ltd.
Whiteshell Laboratories
Attn: B. Goodwin
Pinawa, Manitoba, CANADA R0E 1L0

Francois Chenevier (2)
ANDRA
Route de Panorama Robert Schumann
B. P. 38
92266 Fontenay-aux-Roses, Cedex
FRANCE

Joel Chupeau
National Radioactive Waste Mgmt. Agency
Route de Panorama Robert Schuman
B. P. 38
92286 Fontenary-aux-Roses
Cedex
FRANCE

Jean-Pierre Oliver
OECD Nuclear Energy Agency
Div. of Radiation Protection & Waste Mgmt.
38 Boulevard Suchet
75016 Paris, FRANCE

Claude Sombret
Centre d'Etudes Nucleaires de la Vallee Rhone
CEN/VALRHO
S.D.H.A. B.P. 171
30205 Bagnols-Sur-Ceze, FRANCE

Commissariat a L'Energie Atomique
Attn: D. Alexandre
Centre d'Etudes de Cadarache
13108 Saint Paul Lez Durance Cedex
FRANCE

Bundesanstalt fur Geowissenschaften und
Rohstoffe
Attn: M. Langer
Postfach 510 153
D-30631 Hannover, GERMANY

Bundesministerium fur Forschung und
Technologie
Postfach 200 706
5300 Bonn 2, GERMANY

Institut fur Tieflagerung
Attn: K. Kuhn
Theodor-Heuss-Strasse 4
D-3300 Braunschweig, GERMANY

Gesellschaft fur Anlagen und Reaktorsicherheit
(GRS)
Attn: B. Baltes
Schwertnergasse 1
D-50667 Cologne, GERMANY

Physikalisch-Technische Bundesanstalt
Attn: P. Brenneke
Postfach 3345
D-3300 Braunschweig, GERMANY

Shingo Tashiro
Japan Atomic Energy Research Institute
Tokai-Mura, Ibaraki-Ken, 319-11
JAPAN

Netherlands Energy Research Foundation ECN
Attn: L. H. Vons
3 Westerduinweg
P.O. Box 1
1755 ZG Petten
THE NETHERLANDS

Svensk Karnbransleforsorjning AB
Attn: F. Karlsson
Project KBS (Karnbranslesakerhet)
Box 5864
S-102 48 Stockholm
SWEDEN

Nationale Genossenschaft fur die Lagerung
Radioaktiver Abfalle (2)
Attn: S. Vomvoris
P. Zuidema
Hardstrasse 73
CH-5430 Wettingen
SWITZERLAND

AEA Technology
Attn: J. H. Rees
D5W/29 Culham Laboratory
Abington, Oxfordshire OX14 3DB
UNITED KINGDOM

AEA Technology
Attn: W. R. Rodwell
044/A31 Winfrith Technical Centre
Dorchester, Dorset DT2 8DH
UNITED KINGDOM

Dr. David Read
RM Consultants, Ltd.
Suite 7 Hitching Court
Abingdon Business Park
Abingdon, Osfordshire OX14 IRA
UNITED KINGDOM

AEA Technology
Attn: J. E. Tinson
B4244 Harwell Laboratory
Didcot, Oxfordshire OX11 ORA
UNITED KINGDOM

D. R. Knowles
British Nuclear Fuels, plc
Risley, Warrington, Cheshire WA3 6AS
1002607 UNITED KINGDOM

Internal

MS	Org.	
0827	1502	P. J. Hommert
1324	6115	P. B. Davies
1320	6719	E. J. Nowak
1320	6748	M. D. Siegel (10)
1320	6119	B. Thomson
0750	6118	H. Westrich
0750	6118	P. Brady
0750	6118	H. Stockman
1332	6121	J. R. Tillerson
1395	6700	P. Brewer
1335	6705	M. Chu
1395	6707	M. Marietta
1335	6000	W. Weart
1395	6701	L. Shephard
1341	6706	A. L. Stevens
1328	6749	D. R. Anderson
1395	6743	V. H. Slaboszewicz
1341	6747	D. R. Schafer
1341	6748	J. T. Holmes
1328	6741	H. N. Jow
1330	6352	C. B. Michaels (2)
1330	6352	NWM Library (20)
9018	8523-2	Central Technical Files
0899	13414	Technical Library (5)
0619	12615	Print Media
0100	7613-2	Document Processing (2) for DOE/OSTI